FACULTY OF SCIENCES

Temporal analysis of microglial morphology in mice expressing human Tau with a P301S mutation

Daan Verhaege
Student number: 01306267

Promoter Ghent University: Prof. Dr. Roosmarijn Vandenbroucke

Erasmus promoter: Prof. Dr. Elga de Vries
Scientific supervisor: Dr. Marijn Schouten

Master's dissertation submitted to Ghent University to obtain the degree of Master of Science in Biochemistry and Biotechnology. Major Biomedical Biotechnology

Academic year: 2017-2018

Department: Biomedical Molecular Biology
Vrije Universiteit Amsterdam The Netherlands
Department: Molecular Cell Biology and Immunology

UNIVERSITEIT GENT

Amsterdam UMC
Universitair Medische Centra

VU

Acknowledgements

Research is never conducted alone. Results are never interpreted by a single person and a thesis is never a work realized by a single student. From filling pipet boxes to creating paper-proof images, science relies on teams. I can proudly say that all people involved in conducting this thesis research created one of the best teams I could ask for. First of all, I would like to thank Roos and Griet for giving me the opportunity to prepare my thesis research in Belgium and provide all the support needed for my very first steps in science. I would like to thank Elga for the opportunity to perform my research in the MCBI. I would like to thank the complete Elga De Vries group for the opportunity to present my findings and fruitful discussions thereafter. I would like to thank the student-room members (Lisa, Kyra, Céline, Sophie, Cheyenne, Laura, Marco and Tim) for making every day an enjoyable one and help me explore Amsterdam. I would especially like to thank Céline, Niels and Filip for their expertise on Adobe Illustrator®, Photoshop® and great lay-out comments. I would like to thank my parents for everything they did to make this experience possible. I would like to thank Lulu for her infinite patience, support, care and visits throughout the whole period. Finally, I would like to thank Marijn for the numerous coffee breaks, science facts, jokes, but also his excellent guidance which altogether made the past five months a true joy to work!

Table of Contents

Acknowledgements I

List of Abbreviations III

English Summary V

Part 1: Introduction 1

1.1. Dementias 1
1.2. Frontotemporal dementias 4
1.3. Tauopathy 6
1.4. P301S Mice 10
1.5. Microglia in the dementia brain 13

Part 2: Aim of the Research 18

Part 3: Results 20

3.1. Spatio-temporal expression of phosphorylated tau 20
3.2. Microglial morphology 20
3.3. Temporal expression of phospho tau, Iba1 and CD68 22
3.4. Microglial ramification complexity 24
3.1. Lysosomal volume and content 26

Part 4: Discussion 30

Part 5: Materials and Methods 38

Mice & sample isolation 38
Immunohistochemistry 38
Microscopy 38
Morphological Analysis 39
Statistical Analysis 39

Part 6: References 41

Part 7: Addendum 48

List of Abbreviations

3D-LSS	three-dimensional lysosomal surface simulation
3D-MeSS	three-dimensional merged surface simulation
3D-MSS	three-dimensional microglial surface simulation
3D-PTSS	three-dimensional phospho tau surface simulation
3D-SEM	three-dimensional scanning electron microscopy
AD	alzheimer's disease
APP	amyloid precursor protein
Aß42	amyloid-beta-42
ATP	adenosine triphosphate
AU	arbitrary units
AUC	area under the curve
C1q	complement ligand 1q
C3	complement ligand 3
C3R	complement Receptor 3
CBD	corticobasal degeneration
CD11b	cluster of differentiation 11b
CD68	cluster of differentiation 68
CD90	cluster of differentiation 90
CNS	central nervous system
DAPI	4',6-diamidino-2-phenylindole
DG	dentate gyrus
EMPs	erythromyeloid precursor cells
FTD	frontotemporal dementia
FTDP-17T	frontotemporal dementia with parkinsonism and tau
GRN	granulin
hTau	human Tau
Iba1	ionized calcium binding adaptor molecule 1
IHC	immunohistochemistry
LBD	lewy body dementia
MAP1B	microtubule associated protein 1B
MAPT	microtibule associated protein tau
mGluR	metabotropic glutamate receptors
MHC I/II	major histocompatibility complex I/II
MMPs	matrix metalloproteinases
Mo	months old
mPFC	medial prefrontal cortex
MT	microtubules
NFT	neurofibrilary tangle
No	number of
ns	not significant
Ntg	non-transgenic
OPC	oligodendrocyte precursor cell
P2RY12	purinergic receptor Y12
PBS	phosphate buffered saline
PFA	paraformaldehyde

PHF	paired helical filaments
PiD	pick's disease
PSD95	post synaptic density protein 95
PSEN1/2	presenilin 1/2
PSP	progressive supranuclear palsy
Tau	tubulin associated unit
Thy1	thymocyte antigen 1
WHO	world health organization
YS	yolk sac

English Summary

Many neurodegenerative diseases (such as frontotemporal dementia) are characterized by hyperphosphorylation and aggregation of tau protein resulting in the onset of neurofibrillary tangles (NFTs) followed by neuronal cell death, a process termed tauopathy. The role of microglia herein is unclear. During this master dissertation, we aimed at performing a spatio-temporal analysis of microglial morphology and correlate these with different NFT-loads, and investigate microglial uptake of phosphorylated tau species. To do so, we used Thy1-hTau.P301S mice, a mouse model for tauopathy expressing human mutant tau with a P301S mutation from the neuron-specific Thy1 promoter. We optimized immunohistochemical stainings that allow visualization of microglia, phosphorylated tau and lysosomes in brain sections of P301S- and non-transgenic mice, and imaging was performed through standard fluorescent- or confocal microscopy. For different regions investigated in P301S mice, phosphorylated tau was consistently expressed from 4 months and clear NFT-like structure were visible from 5.5 months of age. We observed a time-dependent reduction in cortical microglial ramification complexity, but differences between genotypes were only apparent at 5.5 months of age as P301S microglia showed a reduced ramification complexity compared to their non-transgenic counterparts. Interestingly, this reduction was independent of the distance towards the closest NFT-like neuron. In these 5.5 months old P301S animals, cortical microglia showed a mild hypertrophy and bigger soma, reminiscent of an activated morphology, compared to a more ramified morphology in non-transgenic animals. Besides a different morphology, 5.5 months old transgenic animals also showed a bigger lysosomal volume inside microglia, indicative of a higher phagocytic activity, compared to their non-transgenic counterparts. Furthermore, inside microglial lysosomes of transgenic animals, we detected a time-dependent increase in relative phospho tau volume and these signals were most frequently observed in lysosomes located distant from the soma and closer towards the end of ramifications. Interestingly, we did not observe microglia engulfing complete neurons, but did see frequent interactions between ramification ends and either neuronal surface or extracellular NFTs (ghost tangles).

Altogether, we observed a changed morphology, increased lysosomal volume and phospho tau signals inside lysosomes of cortical microglia in Thy1-hTau.P301S animals compared to their non-transgenic couterparts, which occurred only after consistent phospho tau expression and NFT onset. Future research should focus on investigating the functional implications of tau uptake by microglia and unravel the beneficial or detrimental roles of microglia in tauopathies.

Part 1: Introduction

1.1. Dementias

"It's the only disease I know of where you're told to go home, get your affairs in order, spend time with your family and die, not fight your life" …

… is probably the most famous sentence written by Kate Swaffer, a writer and poet who was diagnosed with early onset frontotemporal dementia at the age of 49 years old (Swaffer, 2016). Since her diagnosis, Kate tries to raise awareness on living with dementia through speeches, writing, blogging, and currently also leads the Dementia Alliance International, a group aiming to educate people on dementia and fight for individual autonomy (www.dementiaallianceinternational.org). Even the World Health Organization (WHO) acknowledges the lack of awareness on dementias and recently initiated the "Global action plan on the public health response to dementia 2017-2025" (www.who.int, 12 December 2017). Such initiatives aim at reducing the risk of dementia and improving treatment and care through research and innovation. The main motivation for these initiatives is the large numbers of patients suffering from dementias: currently, the WHO estimates 50 million people world-wide have dementia and this number is expected to triple by the year 2050(www.who.int, 12 December 2017). Stunningly, in 2015, the associated worldwide economic burden was estimated to be US$ 818 billion (www.who.int, 12 December 2017). These high costs are a result of the direct medical, but also social costs, as dementia has a strong social impact on the life of patients as well as their families, friends and care-takers. The high number of dementia patients and incredibly high costs for care both form the ultimate rationale to continue research on dementias in the search for a cure. Up until today, there is no such cure that can alter or reverse the disease progression, and this is mainly due to the lack of knowledge concerning the cause and disease progression mechanisms.

The clinical aspects of dementia, however, are well documented and covered by the WHO definition of dementia: "Dementia is a syndrome – usually of a chronic or progressive nature – in which there is deterioration in cognitive function (i.e. the ability to process thought) beyond what might be expected from normal ageing. It affects memory, thinking, orientation, comprehension, calculation, learning capacity, language, and judgement. Consciousness is not affected. The impairment in cognitive function is commonly accompanied, and occasionally preceded, by deterioration in emotional control, social behavior, or motivation." (www.who.int, 12 December 2017). Clinical symptoms are the result of damage to the brain and, more specifically, damage to brain circuits. These circuits are made up of many neurons connected to each other and thus these neuronal circuits link different brain regions to allow all the functions the brain offers. When such circuits are perturbed, this may result in a loss of the function this circuit was responsible for. Fortunately, most brain functions can rely on a huge amount of neuronal circuits to perform the same function, and loss of several of these circuits forms no danger for the overall function. Additionally, the brain shows an incredible plasticity, meaning lost functions can be taken over by other regions over time. For example, the hippocampus is the main brain region responsible for the processing and storing of memories and is often damaged in Alzheimer's disease patients. When damage to a single neuronal circuit in the hippocampus occurs, this will hardly affect the memory processing or

storing function. However, if the damage is so severe that a large portion of circuits is affected or perturbed, this may result in dysfunction and clinical symptoms such as memory loss or difficulties remembering recent events. This idea can be applied to all other brain regions as well. For example, damage to the prefrontal cortex is often associated to behavioral problems, etc. All these clinical symptoms and dysfunctions share a common cause: damage to a brain region. Different types of brain damage exist, of which neuronal cell death is the most well-known. Neuronal cell death itself can again result from different events such as accumulation of toxic protein aggregates, neuroinflammation, oxygen shortage through hypoperfusion or stroke and many others. Most dementias are chronic and slowly progressive through neurodegeneration. Depending on the type of damage, localization and symptoms, one can distinguish multiple dementia types like Alzheimer's disease, vascular dementia, Lewy body dementia, frontotemporal dementia and other rare types of dementia. These dementia types are not excluding and thus multiple types can be present in the same patient. The most frequent causes of dementia are discussed shortly in the following paragraphs.

Alzheimer's disease (AD) is a late-onset, chronically progressive neurodegenerative disease and the most common cause (namely 55%, Figure 1) of dementia (Burns & Iliffe, 2009). Clinically, AD is well-known for its disturbances in short term memory, abrupt changes in behavior, mood swings, depression and self-neglect ultimately leading to death by complications within an average period of 8 years (Burns & Iliffe, 2009)(Brunnström & Englund, 2009). As stated earlier, a frequently affected region is the hippocampus, but degeneration in other regions occurs as well. A typical AD hallmark is the presence of amyloid-beta (Aß) plaques, which are thought to be responsible for neuronal cell death (Kadowaki *et al*, 2005). Another AD hallmark is the hyper- phosphorylation of Tau protein resulting in the production of neurofibrillary tangles (NFTs). Amyloid-beta and NFTs together will result in neuronal cell death and clinical symptoms (Clinton *et al*, 2010).

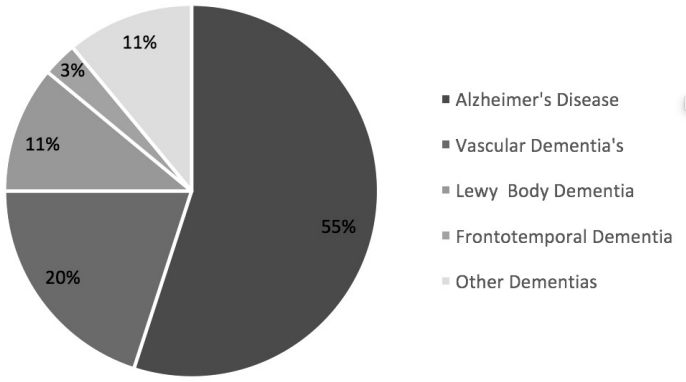


Figure 1. Dementia frequencies. The frequencies (%) are shown relative to the total number of dementia patients (estimated to be 50 million people, WHO, 12 December 2017)

Vascular dementia (VD) is the second most common cause (namely 20%, Figure 1) of dementia (Battistin & Cagnin, 2010). It is usually caused by strokes resulting in hypoperfusion of the brain region that is normally perfused by the affected blood vessels. The hypoperfusion leads to neuronal cell death as neurons are dependent on metabolites and nutrients from astrocytes and oligodendrocytes, which are in turn sensitive to low oxygen levels. Strokes will lead to atrophy of affected regions and thus also clinical symptoms are variable and dependent on the site of injury.

Lewy body dementia (LBD) is the third most common cause (namely 11%, Figure 1) of dementia (Hogan *et al*, 2016). LBD is a synucleinopathy disease, marked by neurodegeneration through intraneuronal accumulation of alpha-synuclein proteins, also

termed Lewy bodies. Up until now, the exact cause for synucleinopathies remains unknown. Affected regions are highly variable and can be part of both the central nervous system (CNS) and autonomic nervous system (ANS), resulting in a wide variety of clinical symptoms. Most frequently, LBD is characterized by extreme visual hallucinations and symptoms associated with PD as tremor, poker face, etc (McKeith *et al*, 2017).

Frontotemporal Dementia (FTD) is a less frequent form of dementia (namely 3%, Figure 1) most known for its neurodegeneration in the frontal or temporal lobes resulting in extreme personality changes and language problems (Finger, 2016), and is discussed thoroughly in the next chapter.

The remaining dementias (together 11%, Figure 1) are very rare and often the dementia is only a side symptom of the slow chronic neurodegenerative character of the disease. In contrast to the chronic nature of all the afore mentioned dementias, non-chronic causes are known as well. For example, hypothyroidism, vitamin B12 deficiency and Lyme's disease are reversible and in some cases treatments are available to speed up the recovery (Carmel, 2008).

The wide variety and complexity of symptoms of the different types of dementias pose a major problem for easy diagnosis and especially differential diagnosis. Therefore, additional criteria, methods and techniques are applied during testing before making a valid diagnosis. As most dementias are chronic and slowly progressive, an important criterion for diagnosis is the minimal duration of symptoms during at least 6 months as this excludes sudden impact events such as trauma (Caplan & Rabinowitz, 2010). Additionally, the potential reversibility of dementias can often be checked through biochemical analysis of the blood. For example, low vitamin B12 levels suggest a reversible type of dementia and not the chronic type (Berg & Shaw, 2013). However, the vast majority of dementias are chronic and the (differential) diagnosis is aided by cognitive testing, imaging and/or biochemical analysis of bio-fluids. Cognitive testing of patients is performed using standardized tests as the mini-mental-state-examination (MMSE) to test attention, memory, calculation, language and other skills. Additionally, people surrounding the patient can be asked about the patient's behavior to aid diagnosis. Structural imaging (via CT scans or magnetic resonance imaging) is often used to assess brain atrophy, whereas functional imaging (e.g. positron emission tomography) can, for example, be used to neuroimage amyloid-beta in AD. Finally, biochemical analysis of blood or cerebrospinal fluid (CSF) can, for example, be used to detect Aß or tau levels to differentiate AD from other dementia types. Currently, the specificity of these different techniques combined is not perfect and many patients are still miss-diagnosed.

Only a very small fraction of the dementia cases is hereditary (Loy *et al*, 2014). The majority are not hereditary, but have been associated with general risk factors as smoking, diabetes, obesity, low education and others (Livingston *et al*, 2017). Risk factors for VD, for example, all affect the blood vessels through smoking, high blood pressure and high cholesterol levels (Livingston *et al*, 2017). Many of these risk factors can be easily prevented through treatment and raising awareness and, therefore, prevention is still an important step in the fight against dementia. When prevention fails, the most important step in fighting any disease becomes the treatment. Unfortunately, there is still no cure available for dementias and current treatments only aim at reducing the symptoms. Currently, management consists of two approaches: 1) psychological therapies aiming to alleviate the social load and 2) medication

to directly target symptoms. The most well-known drug used, was donepezil, an acetylcholinesterase inhibitor that raises acetylcholine levels which are low in Alzheimer's patients due to neurodegeneration of acetylcholine producing neurons (Lee *et al*, 2015). Additionally, other drugs are used to treat the various symptoms associated with the different dementia's. In the last decade, the importance of amyloid-beta and tau in many dementias has become clear and thus antibody therapies are being explored to target the accumulative nature of these pathogenic mechanisms (Schroeder *et al*, 2016). This way, these treatments may be the first to target the underlying disease (progression) mechanisms rather than symptoms. For example, BioArctic currently has a monoclonal antibody targeting soluble and toxic Aß oligomers, which passed clinical phase b2 successfully (www.bioarctic.se). No great progress has been made yet on antibodies targeting tau.

1.2. Frontotemporal dementias

FTD is a group of disorders characterized by neuronal loss in frontal and temporal lobes of the brain. The frontal lobe contains the primary motor cortex and is therefore responsible for planning movements, but also plays a role in reasoning and logical thinking. The temporal lobe contains the primary auditory and visual cortex and thus plays a major role in processing audiovisual cues. Additionally, the area of Broca and Wernicke (the two regions responsible for speech) are located in the frontal and temporal lobes, respectively. Damage (e.g. neuronal cell death) in these brain regions might perturb the associated functions and, therefore, FTD is often associated with behavioral-, speech- and motor deficits (American Academy of Family Physicians. *et al*, 1970). Although the hippocampus also lies within the temporal lobe, it is usually not affected in FTD and therefore memory loss is not a prominent feature of FTD (Snowden *et al*, 2002). These signs and symptoms are used as criteria during the diagnosis and differential diagnosis from AD. Additionally, cortical atrophy in the frontal and temporal lobes is often followed over time to confirm an FTD diagnosis. Multiple types of FTD can be classified based on clinical manifestations and underlying pathological mechanisms or traits. More specifically, FTDs can be sub classified purely on clinical signs and symptoms or, alternatively, sub classified based on pathological features only. The latter cases are referred to as frontotemporal lobular degeneration (FTLD) types. The very first description of FTD was made by Arnold Pick in 1892, who identified dementia in a patient who would currently be diagnosed to have Pick's Disease (PiD), a subtype of FTD (Wang *et al*, 2006). PiD shows a specific pathology through accumulation of tau protein into spherical aggregations (coined Pick's bodies), associated with the degeneration of the frontotemporal lobes. Pick's disease is a pathology example that can result in FTD. Many such variants have been described and, in the last decades, many genetic mutations have been linked to these pathologies as well. However, many identified mutations are not specific for only one pathology or FTD subtype, and a single mutation can result in different disorders within the same family (Bugiani *et al*, 1999). To make matters even more complex, many FTD cases don't show genetic aberrations (Loy *et al*, 2014). Therefore, current classifications of FTD (sub)types rely on the clinical manifestations present and, as such, seven main subtypes are recognized: FTD associated with motor neuron disease, progressive supranuclear palsy, corticobasal degeneration, behavioral variant of FTD, semantic variant primary progressive aphasia, nonfluent agrammatic variant primary progressive aphasia and primary age-related tauopathy.

Familial forms of FTD are common and a wide spectrum of mutations have already been identified in different families. Current state-of-the-art sequencing technologies used in the genetic- and mutation discovery analyses are continuously adding new FTD-associated mutations to the list. Most of the mutation (in)directly result in increased levels of hyperphosphorylated Tau. The exact mechanisms of how these tau species result into neurodegenerative disorders (also coined "Tauopathies"), are described in the upcoming sections. Mutations can be present multiple genes, of which the most frequently mutated are the Microtubule Associated Protein Tau (MAPT) gene and the Granulin (GRN) gene. The MAPT gene is located on chromosome 17 and mutations can result in FTDs belonging to the group of frontotemporal dementias with parkinsonism-17 with Tau (FTDP-17T) or, alternatively, progressive supranuclear palsy (PSP) or corticobasal degeneration (CBD) (Sperfeld *et al*, 1999; Bugiani *et al*, 1999). In terms of classifying FTD subtypes based purely on pathology, MAPT mutation result in cases of FTLD with Tau (FTLD-Tau). For example, in our current study we use transgenic mice expressing human tau with a P301S mutation, which was discovered in FTDL-Tau and FTDP-17T patients. As sub-classification based on clinical signs and symptoms is not possible in animal models, the P301S mice represent cases of FTLD-Tau. Interestingly, the P301S Tau mutation was shown to result in FTDP-17T and corticobasal degeneration in a father and son, respectively (Bugiani *et al*, 1999), again indicating a simple classification based on individual mutations is incomplete and, in human patients, should be accompanied by clinical manifestations. Already more than 40 Tau mutations were discovered that can cause FTDP-17T, such as the P301L (Hutton *et al*, 1998), P301S (Bugiani *et al*, 1999; Sperfeld *et al*, 1999) and R406W (Hutton *et al*, 1998) mutation. The initial symptoms of FTDP-17T patients appear at 40 or 50 years of age and include a general loss of interest and mild speech and language deficits. Behavioral problems manifest as a loss of inhibition, delusions, hallucinations and obsessive compulsive (eating) behavior (Ludolph *et al*, 2009). Additionally, patients develop motor deficits very similar to those of PD patients, including tremor, poker face and walking problems (Ludolph *et al*, 2009). Life expectancy after diagnosis is 5-10 years (www.ghr.nlm.nih.gov). Post-mortem, the brains of FTDP-17T and/or FTLD patients show higher Tau levels and severe frontal lobe atrophy compared to other causes of FTD (Dickson *et al*, 2011). Next to the MAPT gene, also the GRN gene has been associated with FTDs. The GRN gene is expressed to create progranulin, a precursor protein that is cleaved into granulin. Granulin has widespread functions throughout the body and, interestingly, is also responsible for neuronal survival (Ryan *et al*, 2009). Unsurprisingly then, mutations in the GRN gene have been associated with subtypes of FTD (coined GRN-related FTDs) that account for approximately 5-10% of all FTD cases (www.ghr.nlm.nih.gov). The first symptoms in such patients appear at 50 or 60 years of age and are very similar to those of FTDP-17T patients. Additionally, GRN related FTD patients develop problems to carry out purposeful movements and are easily distracted and thus show problems in completing daily tasks or activities (Le Ber *et al*, 2008). Life expectancy after diagnosis is 6-7 years (www.ghr.nlm.nih.gov). Although the different FTD types and variants show different clinical manifestations, they share a common pathological manifestation of hyperphosphorylated Tau species. This does implicate, however, that a single treatment could prove effective against all types of FTD (and potentially other neurodegenerative tauopathies) and therefore more research is required into the exact mechanisms of tauopathy.

1.3. Tauopathy

Neurodegenerative disorders are characterized by neuronal cell death and the associated clinical symptoms are dependent on the specific region of neurodegeneration. Many factors, e.g. oxygen shortage, can induce neuronal cell death. More recently, protein aggregates were found to be very potent inducers of neuronal cell death (Nixon & Yang, 2012). These aggregates are, for example, the result of an overproduction of the aggregating protein, thereby pushing the equilibrium towards aggregated protein conformations instead of the monomeric form. Overproduction itself can result from mutations in the encoding genes which affect the transcription rate, or more indirectly through mutations of genes that have a role in processing the aggregating protein (Goedert & Jakes, 1990). Alternatively, mutations in the genes encoding the aggregating proteins may directly result in altered protein conformations with a stronger ability to stick to one another (Wegmann *et al*, 2011). For example, AD has been associated with mutations in genes encoding for APP (Amyloid precursor protein, the aggregating protein in AD) and PSEN1/2 (Presenilin1/2) which is responsible for cleaving the APP into smaller fragments (O'Brien & Wong, 2011). Mutations in any of these genes can (indirectly) lead to the increased formation of extracellular amyloid-beta plaques (O'Brien & Wong, 2011). Besides these plaques, other types of pathogenic protein aggregations, e.g. consisting of hyperphosphorylated Tau, were found to be associated with neurodegenerative diseases. Later on, mutations in the MAPT gene were identified in patients suffering from hereditary forms of FTD and/or parkinsonism, indicating that Tau dysfunction alone can result in neurodegeneration and dementias (Poorkaj *et al*, 1998; Hutton *et al*, 1998; Spillantini *et al*, 1998). These diseases are often termed primary tauopathies, in contrast to secondary tauopathies (e.g. Alzheimer's disease) where tauopathy is not the only pathological feature. Since then, tauopathy has been found to be a key pathological mechanism in over 25 neurodegenerative diseases (Spillantini & Goedert, 2013). The function of Tau and mechanisms of how soluble and monomeric Tau can develop into hyperphosphorylated and aggregated Tau will be discussed shortly below and are presented in figure 2.

The first description of NFTs was made by Dr. Aloïs Alzheimer in 1907 in post mortem brain tissue sections from the famous patient Auguste Deter (A. Alzheimer, 1907). Since then, it took 81 years until the identity of the aggregating protein was found. This protein that makes up the core of NFTs was coined Tau (tubulin associated unit) (Weingarten *et al*, 1975). Later on, the associated encoding cDNA of Tau was discovered and used to map the MAPT gene on chromosome 17 (Neve *et al*, 1986). A schematic overview of the MAPT gene is shown in figure 2a. The MAPT gene contains 16 exons, from which exon 2, 3 and 10 are subject to alternative splicing (Goedert *et al*, 1989). This way, up to 6 different Tau products can be created. Exon 2 and 3 are located nearby the N terminal projection domain of Tau and are therefore called N-terminal inserts (1N or 2N if only one or both exons, respectively, are included). Exon 10 codes for a repeat region containing a microtubule binding domain. All Tau transcripts contain at least three such repeat regions (3R), but can have a fourth (4R) if exon 10 is included. Combinations of different inserts are indicated using the short abbreviations, e.g. 4R/2N contains exon 2, 3 and 10 and thus forms the larges isoform of 441 aminoacids. Many transgenic animal models, such as the Thy1-hTau.P301S mice used in our current study, express the 4R/0N isoform of 383 aminoacids. In the adult human brain, there is a balance in 4R and 3R products (Goedert & Jakes, 1990).

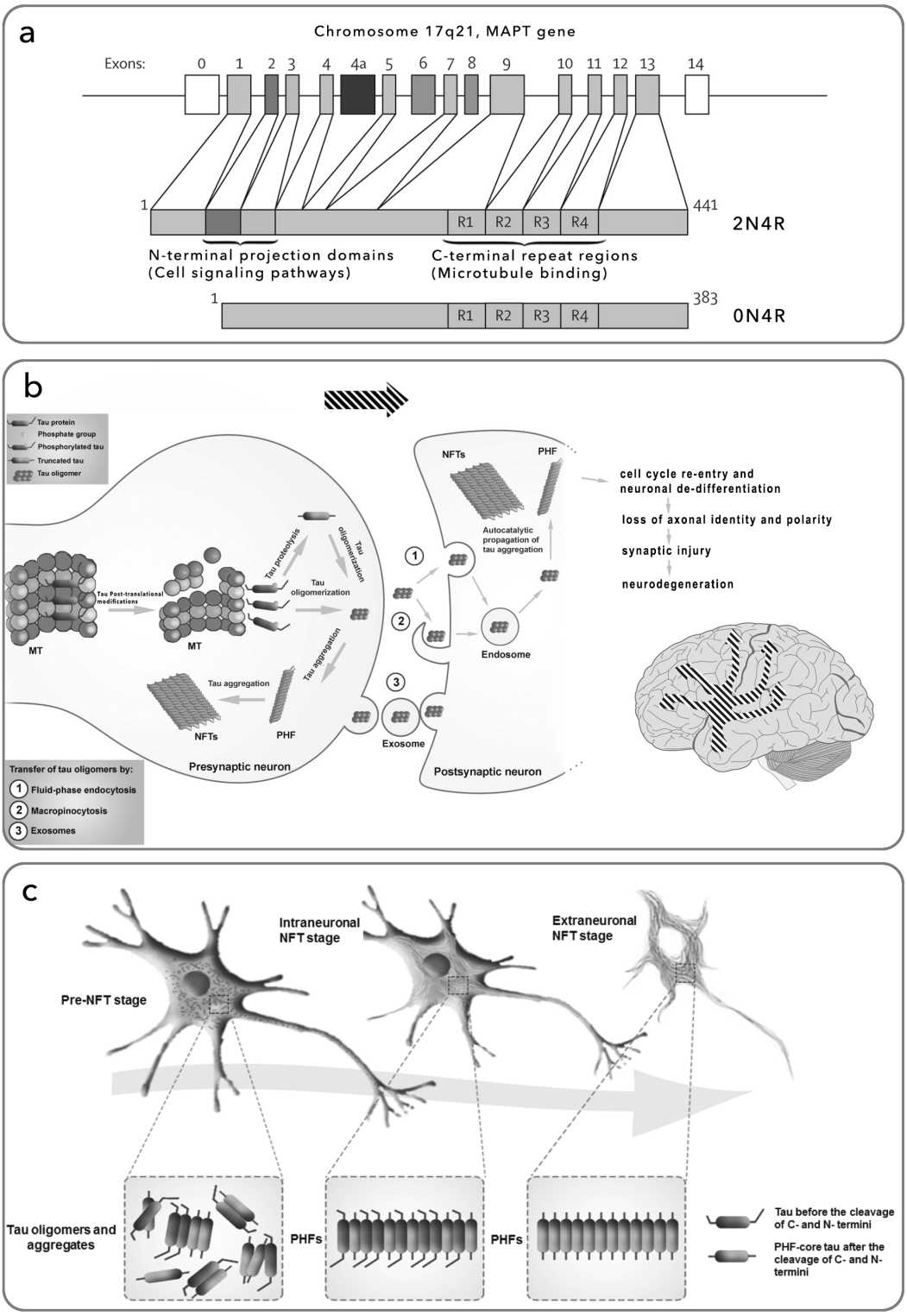


Figure 2. Tauopathy in human brain diseases. a) Schematic overview of the MAPT gene, showing the different exons and two possible transcripts thereof after alternative splicing. As an example, the 2N4R and 0N4R transcripts are shown (and not the 1N4R, 2N3R, 1N3R nor 0N3R) (figure adapted and modified from (Spillantini & Goedert, 2013)). b) Schematic representation of tau functions and post-translational modifications resulting in PHF and NFT formation, as well as tau transport mechanisms. Earliest tau aggregates are found in the temporal lobe and spread towards the cortex (striped arrows on the brain) (figure partly adapted and modified from (Šimić *et al*, 2016)). c) Different stages of NFT formation are showed with indications of how PHFs are composed on a molecular level. Over time, more cleavage and phosphorylation of tau occurs (figure adapted and modified from (Šimić *et al*, 2016)). MT: microtubules. PHF: paired helical filaments. NFT: neurofibrillary tangle.

Once expressed, the natively unfolded, monomeric and soluble Tau protein will associate with microtubules (in neuronal axons), through binding of the repeat regions and function as stabilizer and aid microtubule assembly (Cleveland *et al*, 1977a, 1977b). Microtubules are especially important in neurons as they help form the long-shaped cells and are responsible for axonal transport of a range of molecules, protein complexes and even organelles. This stabilization and assembly function is dependent on repeat regions (located in the C-terminal half of Tau protein) facilitating microtubule binding. Additionally, Tau contains an N-terminal projection domain capable of binding kinases and other protein complexes and, through these interactions, tau has been associated to have a role in cell signaling (Morris *et al*, 2011), long term potentiation (Ahmed *et al*, 2014), heat stress response (Sultan *et al*, 2011) and autophagic clearance (Leyk *et al*, 2015). Interestingly, Tau is probably not the major protein responsible for microtubule assembly and stabilization, since heterozygotic Tau knock-out animals show no altered phenotype (Dawson *et al*, 2001; Harada *et al*, 1994). Contrarily, microtubule associated protein 1B (MAP1B) is considered the prime microtubule stabilizer and assembler that works in complement with MAPT/Tau. This idea was confirmed in MAP1B knock-out animals, which do show abnormal development and neurodegeneration (Takei *et al*, 2000). Interestingly, these findings bring about the question if reduced microtubule stabilization though tau mutation/hyperphosphorylation actually is a driving pathological mechanisms in both AD and FTLD.

As stated earlier, the natively unfolded tau protein binds to microtubules. However, many post-translational modifications are known to prohibit these interactions. Examples are phosphorylation (Jameson *et al*, 1980), acetylation (Kingwell, 2015) and enzyme-mediated cleavage (Harrington *et al*, 2015). Phosphorylation of residues nearby the repeat regions can directly reduce the microtubule-binding capacity or, alternatively, favor tau-tau interactions instead, moving the equilibrium towards tau aggregate formation. However, not all tau phosphorylation sites are associated with pathological interactions. Many residues are always phosphorylated in healthy conditions, whereas some of these go missing in pathological conditions. The opposite situation -where more sites and novel residues are phosphorylated, a situation called hyperphosphorylation- is a better known phenomenon ultimately leading to tau aggregation. Additionally, also enzyme-mediated cleavage has been shown to promote an “auto-catalytic process” leading to tau aggregation. More specifically, two cleavage sites in the tau protein can be used by several proteases to create the F3 unit; a truncated tau fragment containing only the repeat regions. The F3 unit is able to bind native unfolded tau and induce a similar C-shaped conformation that is proteolytically stable but more prone to phosphorylation. Therefore, a single cleaved F3 fragment can generate additional F3 fragments by binding native Tau proteins in an auto-catalytic manner very similar to the spread of prion proteins (Harrington *et al*, 2015). These C-shaped fragments favor tau-tau interactions over tau-microtubule interactions resulting in aggregation (Lee *et al*, 1991). These tau aggregates can combine to create a paired helical filament (PHF), with a core made up of the C-shaped fragments and a fuzzy coat created by incorporated non-truncated tau molecules (Wang *et al*, 2009). Not all tau molecules in PHFs are truncated, but as PHFs develop, the truncated species become more frequent. Residues residing in the fuzzy coat are more prone to phosphorylations as well. As more PHFs are created and clump together, the neuron develops through multiple stages. The first stage is called the pre-tangle stage and is characterized by the start of PHF build-up without neuronal dysfunction. Later on, during the intra-neuronal stage, the neuron is almost completely filled with PHFs that dysregulate

neuronal function. Such neurons are referred to as NFTs. In a final stage, when NFTs die, the tau aggregates remain in the extracellular environment and these tangles, in the extraneuronal stage, are then called ghost tangles. Such ghost tangles, however, are not present in all tauopathy associated neurodegenerative diseases. For example, ghost tangles are found in tissue sections of FTDP-17T and FTLD patients, but not of patients suffering from corticobasal degeneration (Ishizawa & Dickson, 2001). Additionally, in some neurodegenerative tauopathies, the tau aggregates are also present in other types of aggregates besides the NFTs. For example, Pick's disease is characterized by the presence of pick's bodies, which are swollen neuronal inclusions.

In patients with hereditary forms of FTD, for example, all neurons express a pathological Tau protein ultimately leading to tau aggregation, NFT formation and finally neurodegeneration throughout the whole brain. Nonetheless, there seems to be a trend in Tau aggregation in specific brain regions at different stages of disease. The earliest tau aggregates are found in the limbic system of the temporal lobe. From this site, aggregates seem to emerge or spread towards the centers of Wernicke and Broca, the frontal lobes and only then spread towards the primary motor and sensory areas residing in the cortex. Interestingly, also patients with non-familial forms of FTD show these patterns of tau aggregation, indicating tau aggregates originating in single cells (by currently unknown mechanisms) can spread or be transported towards other neurons throughout the whole brain in a manner very similar to the spread of prion proteins (Hall & Patuto, 2012). It is currently unclear why temporal neurons are more sensitive to tauopathy and show the earliest signs of tau aggregation. Independent of the brain region, most of the aggregated tau species are present in the axons and synapses of neurons. From the synapses on, tau species can be propagated between neurons through secretion of exosomes (Saman *et al*, 2012; Wischik *et al*, 2014) or, alternatively, trans-synaptically through direct secretion (Wischik *et al*, 2014; Le *et al*, 2012) and can be taken up by the healthy post-synaptic neuron through micropinocytosis (Holmes *et al*, 2014) or clathrin-mediated endocytosis (Rubinsztein, 2006). Interestingly, in AD patients, the spread of tau aggregates, rather than the spread of amyloid-beta plaques, correlates with the clinical manifestations, again indicating tauopathy is of major importance in neurodegenerative diseases and a potential therapeutic target. To this end, multiple approaches are currently being tested; inhibition of tau phosphorylation (Le Corre *et al*, 2006; Varghese *et al*, 2014), proteolysis and aggregation (Wischik *et al*, 2014). On the contrary, promoting the intracellular and extracellular tau clearance is also being explored (Berger *et al*, 2006; Troquier *et al*, 2012).

Neuronal cells accumulating tau aggregates are characterized by neurodegeneration in the long term. The exact mechanisms and pathways responsible for inducing neuronal cell death are unknown, but some observations have paved the way for further research. One of the first associated events aiding in the process is the activation of genes involved in cell cycle re-entry and neuronal de-differentiation (Wang *et al*, 2007; Andorfer *et al*, 2005; Ambegaokar & Jackson, 2011; Stone *et al*, 2011). Additionally, executioner caspases are upregulated and reactive oxygen species are produced, but no signs of classical apoptosis are present (Müller *et al*, 2010; Swerdlow & Khan, 2004). Altogether, these events were shown to lead to a loss of axonal identity and polarity, ultimately leading to synaptic injury. The role of other cells (e.g. microglia) assisting in the neurodegeneration remains unclear.

1.4. P301S Mice

The exact mechanisms of how individual Tau mutations can lead to neurodegeneration are still unclear (Gasparini *et al*, 2007). As a result, animal models of tauopathy have been developed to study these mechanisms in more detail. Such models are based on genetic mutations identified in patients suffering from hereditary forms of AD, FTD and many other chronically progressive neurodegenerative diseases. As mentioned earlier, FTDP-17T and FTLD are frequent form of FTD characterized by tauopathy. FTDP-17T has been associated with more than 40 mutations in the MAPT gene and some of these have been explored to create transgenic mice overexpressing the human mutated tau gene. Currently, three tau mutations are explored extensively in transgenic mice: R406W (Tatebayashi *et al*, 2002), P301L (Lewis *et al*, 2000) and P301S (Allen *et al*, 2002). The P301L and P301S animal models show features very similar to FTLD patients, but the onset of symptoms and histopathological changes appear earlier in the P301S mice, making them practically more feasible. The different mutated genes are inserted into the mouse genome and can be expressed from different promoters. For example, the P301S mice created by Yoshiyama *et al* overexpress human tau with a P301S mutation from the mouse prion protein (MoPrP) promoter (Yoshiyama *et al*, 2007). Therefore, transgene expression is detected in most cell types throughout the whole brain. Interestingly, human tauopathy brains show strong NFT formation, but tau aggregates were also found inside a minority of microglia (Bugiani *et al*, 1999). Therefore, mice expressing human mutant tau in neurons and microglia (e.g. the MoPrP-hTau.P301S mice) seem to reflect the human situation to a large degree. The overexpression of human mutant tau in microglia, however, might be extravagant compared to the human situation. Additionally, this overexpression might be disturbing when aiming to investigate the role of microglia in tauopathies. Contrarily, Allen *et al* (2002) created a similar transgenic line using the murine Thymocyte antigen 1 promoter (also called the cluster of differentiation 90; Thy1 and CD90, respectively) (Allen *et al*, 2002). The Thy1 antigen was the very first marker identified for T cells (Reif & Allen, 1964). Since then, it has been studied extensively and has been incorporated as a standard neuron-specific promotor to drive transgene expression in the nervous system (Feng *et al*, 2000). An overview of the P301S mice and their characteristics is shown in Figure 3. The response of microglial cells towards neurofibrillary tangles is still unclear and therefore, in the current study, the Thy1-hTau.P301S transgenic mice line was used as a model to address the research question.

The Thy1-hTau.P301S (CBA.C57BL/6) transgenic mice line was created by the group of Prof. Michel Goedert at the Medical Research Council Laboratory of Molecular Biology (University of Cambridge, United Kingdom) (Allen *et al*, 2002). Site-directed mutagenesis was performed to create the P301S mutation into a cDNA coding a four-repeat tau isoform. More specifically, the isoform is 383 amino acids long and has four microtubule-binding domains and lacks N-terminal inserts, therefore called “4R/0N”. This cDNA was then subcloned into a Thy1 expression vector and micro-injected into embryos of mixed background (CBA/ca x C57BL/6J). Founders were intercrossed with C57BL/6J mice and homozygotic mice were analyzed extensively. Currently, the site of genomic integration of the transgene is unknown (www.informatics.jax.org). They used various immunoblotting approaches to show that the human Tau is strongly expressed in spinal cord and brain regions as the cerebral cortex, amygdala, dentate nucleus of the cerebellum and brain stem. The Tau protein localization/distribution within the different brain regions was investigated through

immunohistochemical analysis of 5 months old transgenic mice. Using multiple antibodies, the group showed strong and specific Tau labeling of complete neurons throughout the brain and strongest labeling in the brain stem and spinal cord. Additionally, these experiments showed that the anti-phospho-Tau antibody AT8 (pS202/pT205) shows the strongest and most specific labeling of phosphorylated Tau species in neurons and thus the AT8 antibody is the best option for hTau research in the P301S model mice. For example, the AT8 antibody was also used during immuno-electron microscopy experiments to investigate the filament forming potential of hyperphosphorylated hTau in these P301S mice. The human Tau proteins were shown to be able to form abnormal filaments throughout the soma and processes of neurons. The majority of filaments show ribbon-like structures, are not membrane bound and appear randomly oriented. The minority showed paired helical filament conformations typical for Tau filaments of AD patients. Altogether, Allen *et al* were able to create a mice model for tauopathies in general and FTD, based on the human Tau gene with the P301S mutation. These mice show the major human tauopathy features as neurodegeneration and formation of tau filaments from hyperphosphorylated tau. Unfortunately, these mice do not completely mimic the human situation since, in these mice, no Tau positive glial cells were detected whereas this is the case for human patients with the P301S mutation (Bugiani *et al*, 1999). Additionally, Tau P301S humans show very specific patterns of neurodegeneration which were not specifically detected in the P301S mice.

Noteworthy, and before discussing major findings in P301S animals, it is important to consider the effects of overexpressing a human protein in mice. The overexpression of any protein - even human wild type tau- might result in immune- or other responses in mice. Therefore, when using P301S mice, the ideal control mice would be mice overexpressing human wild-type tau from the same promoter. For example, the ALZ17 mouse line expresses wild type human tau from the murine Thy1 promoter. Feng *et al* have shown that overexpression of wild type tau in mice only results in very low NFT counts and no immune response is apparent (Feng *et al*, 2000). Additionally, Belluci *et al* observed microglial activation in Thy1-hTau.P301S mice but not in the ALZ17 mice, again indicating specific observations in P301S mice are not merely a result of overexpressing human proteins (Bellucci *et al*, 2004). Additionally, these reports suggest that the use of wild-type or non-transgenic mice (as we used in our current study) as control for P301S mice is justified.

Research focusing on neurodegeneration in the P301S model is increasing steadily. Allen *et al* were the first to describe neurodegeneration as they detected severe neuronal loss in the ventral grey matter of the spinal cord, but not in the substantia gelatinosa (Allen *et al*, 2002). Furthermore, they also found that neurodegeneration was associated with reactive astrocytosis and not neuronal apoptosis. Other groups have investigated neuronal loss in the cerebrum and found an age- and layer-specific loss of superficial cortical neurons, but not of neurons in deeper layers (Hampton *et al*, 2010). Other groups have speculated widespread neurodegeneration (and neuroinflammation) in the P301S mouse brain and spinal cord, based on the detection of neuronal COX-2 overexpression (Bellucci *et al*, 2004) since this event was already shown to induce neurodegeneration (Andreasson *et al*, 2001). Interestingly, all studies report 5 months as the youngest age possible to detect neurodegeneration. As an opposite example, no neuronal loss nor apoptosis markers were observed in retinal ganglion cells of P301S mice (Gasparini *et al*, 2011). Altogether, these reports indicate that different neuronal cell populations show different vulnerabilities

towards tauopathy mechanisms and more studies will be needed to investigate how different neuronal cells (or even brain regions) respond to tau dysfunction. In these mice, microglial activation and astrocytosis was observed from 5 and 6 months old on, respectively, which will be discussed later in this introduction.

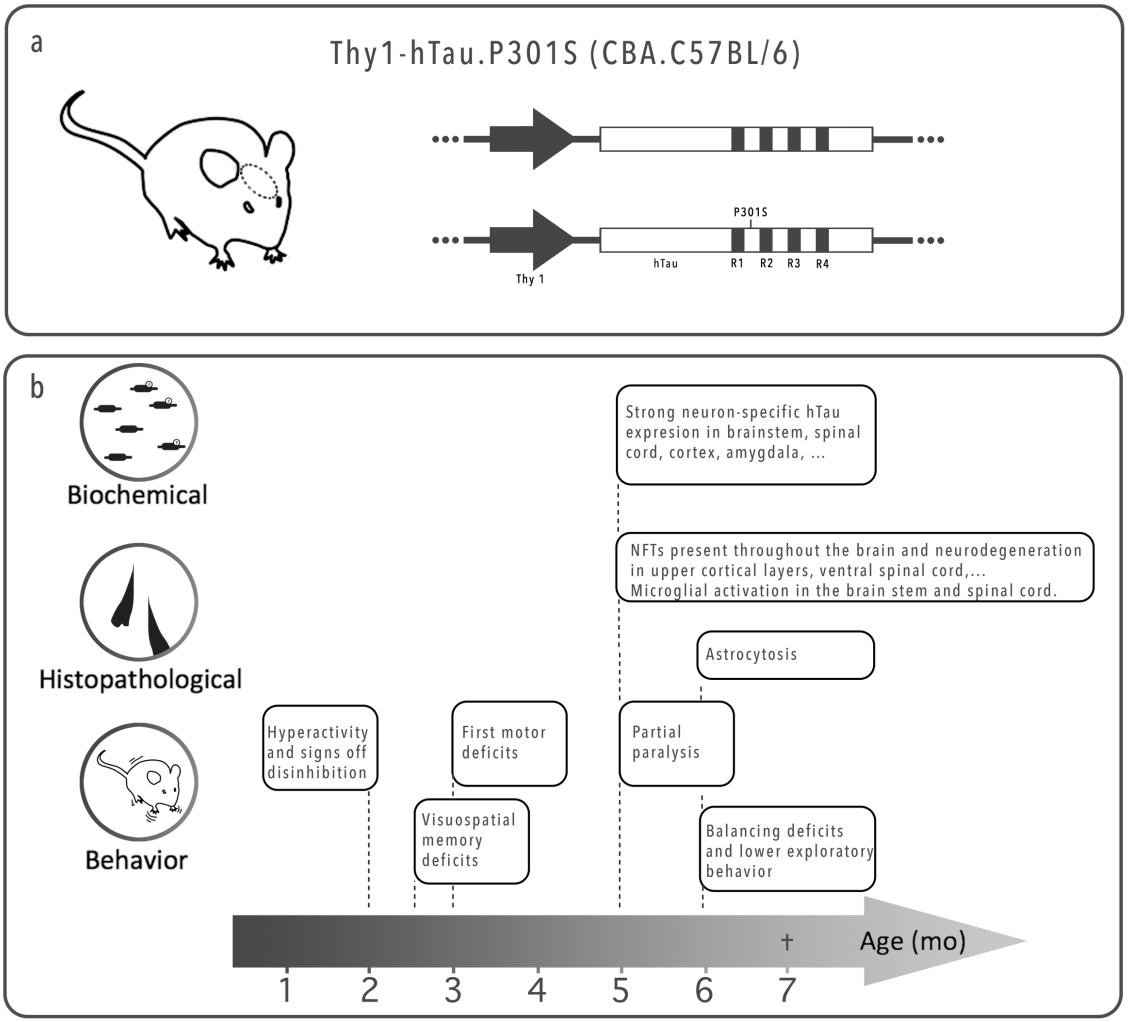


Figure 3. Thy1-hTau.P301S mice as a model for FTD. a) Schematic overview of the integrated transgene construct, consisting of the neuron specific Thy1 promoter followed by the hTau gene (with 4 tau-binding repeat regions and no N terminal insert, coined 4R/0N) with the P301S mutation. b) Timeline showing the biochemical, histopathological and behavioral traits characterized in this model so far. Most animals die at 7 or 8 months old. R1/2/3/4: microtubule-binding repeat region. Mo: Months old.

Finally, the first attempts have already been made to alter the tauopathy progression in P301S mice. Such proof-of-concept experiments aim at opening new avenues for the development of therapeutic approaches for tauopathies. Ozelik *et al*, for example, have shown that treatment with Rapamycin (an FDA approved drug that stimulates autophagy) results in fewer cortical tangles, less tau hyperphosphorylation and less insoluble tau in the forebrain (Ozcelik *et al*, 2013). Interestingly, these effects were accompanied by reduced astrogliosis. Chai *et al* have explored the therapeutic potential of passive immunization in P301S mice with anti-Tau antibodies (Chai *et al*, 2011). They observed a reduced tau pathology, less neurodegeneration and a delayed onset of motor symptoms. As continuously more altered mechanisms are

discovered in animal models of tauopathy, the therapeutic potential of targeting these new mechanisms should also be explored in search for an effective cure.

The histopathological alterations present in the Thy1-hTau.P301S (CBA.C57BL/6) transgenic mice line are accompanied by behavioral deficits, compared to age-matched control mice. Several tests are available to investigate specific behavioral traits. For example, the Morris water maze test is used to investigate memory and spatial learning (Bromley-Brits *et al*, 2011). The ability to stay in balance during movements can be analyzed with the rotarod test (Shiotsuki *et al*, 2010) and the novel open field test can be used to monitor the locomotor- and exploratory activity (Seibenhener & Wooten, 2015). Usually, the whole battery of tests is performed to characterize newly created mice lines. The first symptoms to appear in P301S mice are hyperactivity and signs of disinhibition at two months of age (Scattoni *et al*, 2010). The first cognitive abnormalities arise at 2,5 months, and not earlier (Hickey *et al*, 2005). More specifically, visuospatial memory deficits were found to be correlated to the density of dendritic spines of hippocampal pyramidal neurons (Xu *et al*, 2014). At three months of age, motor deficits become apparent and these evolve over time becoming so sever at five months of age that some animals show signs of partial paralysis of the lower limbs. At six months of age, the animals also show balancing deficits and lower exploratory behavior (Xu *et al*, 2014). Altogether, these early symptoms indicate that behavioral abnormalities are already present before the onset of neurodegeneration (Scattoni *et al*, 2010) and some deficits may even be present before the presence of NFTs. Such phenomena have also been described in mouse models for other neurodegenerative diseases (Littin *et al*, 2008; Hickey *et al*, 2005). Altogether, the Thy1-hTau.P301S (CBA.C57BL/6) transgenic mice line shows symptoms comparable to those seen in FTDP17 patients and these similarities support the use of P301S mice as models to further investigate disease mechanisms. Additionally, the early symptoms described can be used as markers of pathology and as read-outs during validation of new treatments.

1.5. Microglia in the dementia brain

Microglia are the brain-resident immune cells responsible for initiating the innate immune system in order to maintain normal brain homeostasis. Last decades, it became clear these glial cells perform more functions -besides solely scanning the brain parenchymal environment with their long, branched processes- and have been implicated in diseases as AD, PD and tauopathies (Li & Barres, 2017; Mosher & Wyss-Coray, 2014). The development, roles in health and disease and current methods to investigate microglia will be discussed shortly. The morphology, functions and current insights of microglia are shown in figure 4.

The origin of microglial cells has long been unknown since there seem to be no *sensu stricto* adult microglial stem cells present anymore in the adult body. Controversially, the presence of microglial progenitors was observed by several groups, but their origin as well remains unclear (Han *et al*, 2017; Réu *et al*, 2017; Elmore *et al*, 2014). Only very recently different groups were able to pinpoint that microglia originate from yolk sac (YS) cells, more specifically from YS erythromyeloid precursor (EMPs) cells (Kierdorf *et al*, 2013; Gomez Perdiguero *et al*, 2015). During development of the CNS, these EMPs differentiate into YS macrophages (in the cephalic mesenchyme) that migrate and colonize the complete brain (Kierdorf *et al*, 2013; Gomez Perdiguero *et al*, 2015). The exact migration mechanisms are not completely understood, but several observations suggest these YS macrophages are transported over

long distances via the blood (Ginhoux *et al*, 2010), and chemotactic mechanisms are used to further guide the cells towards their final destination inside the central nervous system (Xu *et al*, 2016; Casano *et al*, 2016). Once arrived, the CNS signals these macrophages to differentiate into immature microglia (with specific functions, as discussed below) showing an amoeboid morphology (Ginhoux *et al*, 2010; Kierdorf *et al*, 2013). Amoeboid refers to a ball-like shape, where the cell soma is big and round with very few and short processes. Still early in development, these immature microglia shift their amoeboid morphology to a more ramified one, with long and branched processes. Further maturation of microglia continues while the embryo is developing and microglia are ought to be mature only two weeks after birth (Bennett *et al*, 2016; Butovsky *et al*, 2014). As mentioned earlier, no microglial stem cells have been detected so far, and the observation of microglial proliferation suggests microglial cells are long-lived and the microglial population is maintained through proliferation (Askew *et al*, 2017). Interestingly, the rate of proliferation initially is high, but drops after birth and is region-dependent (Bennett *et al*, 2016). This is consistent with other reports showing microglia show different transcription profiles depending on the specific brain region they are residing (Grabert *et al*, 2016). Additionally, microglia also show different region-dependent responses (in form of transcriptomic profiles) towards aging or acute insults (Galatro *et al*, 2017). Noteworthy, microglial cells are not solely originating from YS-EMPs and were, in rare cases, found to be originating from hematopoietic stem cell-derived monocytes or fetal liver monocytes (Askew *et al*, 2017). It is currently unclear if these microglia show altered functions due to their different history. Altogether, these data suggest the microglial population is very heterogenic and more research is needed to discern different subpopulations and their roles in health and disease.

Mature microglia show a ramified morphology and use the long processes to scan their direct environment, making contact with all CNS cells and matrices. The shape and morphology of microglia can be studied in stainings visualizing microglia-specific markers like the ionized calcium binding adaptor molecule 1 (Iba1), which is (almost) exclusively expressed on microglia and macrophages in unchallenged and activated status. In healthy conditions, almost no macrophages are present in the brain parenchyma, Iba1 stainings therefore show almost exclusively microglia. In neurodegenerative contexts, however, macrophages may potentially infiltrate and therefore also stain positive for Iba1 (Polfliet *et al*, 2002). Other markers often used in microglial research are the major histocompatibility complex II (MHC-II) (Walker & Lue, 2015) and cluster of differentiation 11b (CD11b) (Jeong *et al*, 2013). However, some reports have indicated MHC-II and CD11b expression to increase in activated microglia, suggesting these markers are less suited to show the complete heterogenic microglial population in brain tissue (Sierra *et al*, 2010).

The processes of microglia often contain strong surface receptor expression to recognize specific stimuli and react properly (Tremblay *et al*, 2011). As such, microglia have been implicated in a broad range of functions. A summation of all functions microglia have been associated with, is shown in figure 4. Microglia are most known for being the prime macrophages of CNS parenchymal tissue and thus protect the brain from most pathogens through phagocytosis. In these cases, local inflammation induced by the pathogen also activates microglia which phagocytose the pathogen, infected cells or remaining apoptotic debris (Neumann *et al*, 2008). The process of microglia becoming activated is usually referred to as microgliosis. Morphologically, activated microglia look more hypertrophic and have a

small reduction in ramification complexity. They will phagocytose or engulf material close to the soma and will not use the processes termini. Interestingly, unactivated or unchallenged microglia are also capable of phagocytosing (for example) newly-born neuronal precursor cells in the subgranular zone of the dentate gyrus (Sierra *et al*, 2010). Therefore, controlling the rate of neurogenesis (in both embryonic and adult situations) is also one of microglial cells many functions. Interestingly, unchallenged microglia phagocytose particles near the end of the glial processes, characterized by "pouches" (Figure 4). These pouches can be located at the terminus of the process or form ball and chain-like structures (Sierra *et al*, 2010). In the postnatal brain, most neurons are characterized by the high number of synaptic contacts they make, whereas this is a lot lower in the adult brain. Microglia were shown to be responsible for eliminating the excess of synaptic contacts through a mechanism now termed synaptic pruning (Katz & Shatz, 1996; Hua & Smith, 2004; Huberman *et al*, 2008; Paolicelli *et al*, 2011; Tremblay *et al*, 2010; Stevens *et al*, 2007; Schafer *et al*, 2012). The engulfment of synapses is initiated when the complement receptor 3 (C3R) on microglial processes is triggered by complement ligands C1q and C3, usually present on the surface of weak/extranumerary synapses (Carroll, 2004; van Lookeren Campagne *et al*, 2007; Schafer & Stevens, 2010). During development and throughout the adult life, microglia aid the organization of neuronal networks by directly contacting dendrites, but also through secreting matrix metalloproteinases (MMPs) to help shape an ideal extracellular environment (Nakanishi, 2003). This function was shown to be experience-dependent, indicating microglia are capable of sensing neuronal activity. For example, microglial cells were able to respond to neuronal ATP release through activation of the purinergic (P2RY12) receptor (Dissing-Olesen *et al*, 2014). Besides aiding the development of neuronal contacts, microglia are also capable of modulating the neuronal activity of mature neurons, potentially indirectly through activating astrocytes which in turn release glutamate that can bind metabotropic glutamate receptors (mGluR) on the neuronal surface (Tremblay *et al*, 2011; Pascual *et al*, 2012). Noteworthy, microglial cells are present in the brain before the arrival of neurons, astrocytes and oligodendrocytes (Li & Barres, 2017). As such, they can influence/aid the development of the other CNS cells. For example, microglia were found to guide the positioning of neocortical interneurons towards the 5^{th} cortical layer (Pont-Lezica *et al*, 2014). Many other examples of prenatal and perinatal functions of microglia exist, again highlighting their broad range of functions throughout the complete life (also shown in figure 4).

Most of the functions attributed to microglia were discovered in controlled settings where microglia were depleted or chemically (in)activated. The role of microglia in disease, however, is much less understood. In many diseases or acute insults, microglia change their ramified morphology to a more amoeboid one coinciding with higher phagocytic- and secretory activity of cytokines and/or chemokines (Rock *et al*, 2004). This morphology is now refered to as an "activated" morphology. As such, researchers had hypothesized microglia can show two types of responses towards insults, namely an M1 (pro-) and M2 (anti-inflammatory) phenotype (Tang & Le, 2016). Recent research has, however, shown that the distinction in M1 and M2 does not properly describe the heterogeneity of microglial responses and therefore a spectrum-based nomination is more correct (Galatro *et al*, 2017; Grabert *et al*, 2016). As such, microglial activation (of any kind and any intensity within the spectrum) has been associated with all neurodegenerative diseases (Colonna & Butovsky, 2017; Ransohoff, 2016). The specific contribution of microglia in pathology is dependent on the disease or type of insult. In case of mild inflammatory insults, for example, microglia initiate an injury-

associated ATP release to promote inflammation and initiate a wound-healing response (Davalos *et al*, 2005; Haynes *et al*, 2006; Streit *et al*, 2009). In multiple sclerosis, microglia were also attributed a protective function as they aid the clearance of myelin debris (Yamasaki *et al*, 2014). The roles of microglia in aging and AD, however, remain unclear. For example, in the (healthy) aging brain, dystrophic microglia are apparent (Streit *et al*, 2009). These cells are de-ramified, spheroidal, gnarling and show fragmented processes. The functional implications of this morphology are still unknown, but microglia with an activated morphology are not necessarily more active and dystrophic-looking microglia may just as well phagocytose pathogens. In other words, microglial morphologies don't cancel out the different functions of microglia. In AD, microglia have been associated with tangles (Cras *et al*, 1991). More specifically, in those studies, microglia only seem to associate with extracellular NFTs and not intraneuronal tangles, suggesting microglia phagocytose neuronal debris but not the insoluble, protease resistant filaments. Proof-of-concept for microglia phagocytosing tau species was provided by Luo *et al*, who showed that mouse microglia can internalize and degrade hyperphosphorylated pathological tau species (isolated from human AD brains) *in vitro* (Luo *et al*, 2015). The same microglia were also able to degrade free tau species released from brain tissue sections of Thy1-hTau.P301S mice. Similar observations were made when human brain tissue sections were used. Not much later, Bolos *et al* showed that healthy mouse microglia can phagocytose tau isolated from AD brains and injected in the mouse brain. Additional *in vivo* phagocytosis observations were also reported in marmosets, a non-human primate (Rodriguez-Callejas *et al*, 2016). Later on, researchers were able to show that cortical microglia mimic the regional distribution of NFTs in both AD and healthy controls (Sheffield *et al*, 2000). Interestingly, Streit *et al* have observed that, in the brain of Alzheimer's patients, microglia associated with NFTs show a dystrophic morphology (senescent), rather than an activated morphology (Streit *et al*, 2009). Contrarily, amyloid-beta plaques alone were associated with ramified microglia, indicating the presence of NFTs may cause the dystrophic morphology. However, the dystrophic morphology was also observed in brain areas where neurofibrillary degeneration had not yet spread towards. Altogether, these data suggest that, in aging and Alzheimer's disease, microglia have a neuroprotective role and loss of microglia may result in onset of neurodegeneration. How the loss of microglia is initiated, is unknown. Contrarily to this idea, microglial cells were also found to be capable of spreading tau through exosomes (Asai *et al*, 2015), thus suggesting microglial cells are detrimental and may perhaps aid in the initiation and propagation of tauopathies. In this line, microglial activation was also observed before the onset of NFTs in a mouse model of tauopathy (Yoshiyama *et al*, 2007). However, in this mouse model, hTau with a P301S mutation is expressed in neurons and glial cells, indicating that microglia could be activated by its own hTau expression. Differences between human and rodent brains, alzheimer's disease and pure tauopathies and expression differences between mouse models currently keep the field blurred. To summarize, the role of microglia in neurodegenerative diseases with tauopathies are unclear.

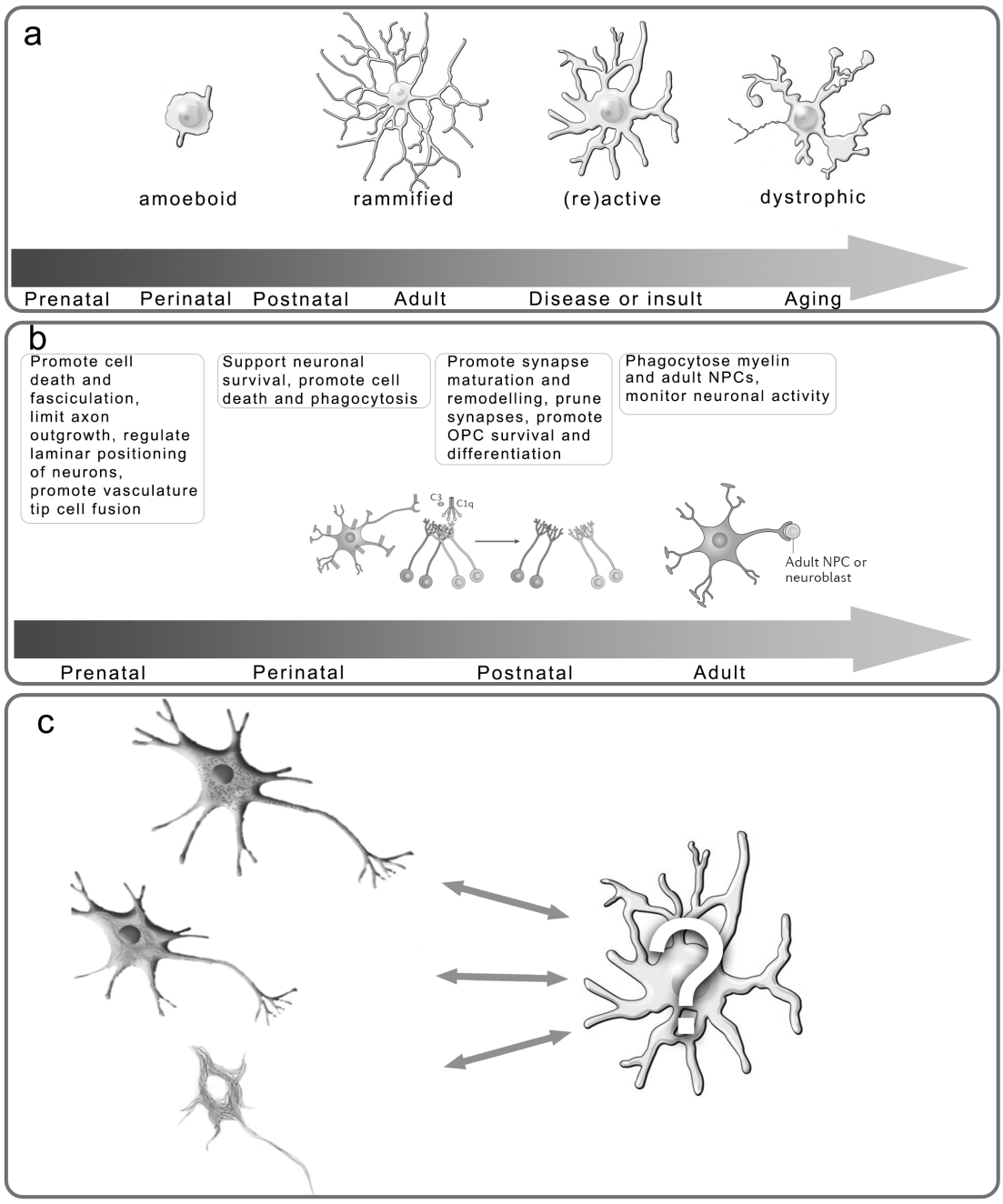


Figure 4. Microglia in brain homeostasis and disease. a) Microglial morphology changes during development and reacts to disease, acute insults and aging (adapted and modified from (Ransohoff, 2016)). Amoeboid refers to a ball-like shape, where the cell soma is big and round with very few and short processes. Ramified microglia have many long and branched processes actively scanning their environment. Ramified microglia phagocytose from the process terminus on. Reactive or activated microglia show a small reduction in ramification complexity and signs of hyperthrophy. Activated cells phagocytose particles from the soma on. Dystrophic microglia are de-ramified, spheroidal, gnarling and show fragmented processes. b) summation of functions that have been attributed throughout development and adult life (adapted and modified from (Li & Barres, 2017)). As an example, pruning of synapses and phagocytosis of NPCs by unchallenged microglia are shown. The engulfment of synapses is initiated when the C3R complement receptor on microglial processes is triggered by complement ligands C1q and C3. c) The response of microglia towards tau species during different NFT-formation stages (pre-tangle, intraneuronal and extraneuronal NFTs) is unclear (adapted and modified from (Šimić *et al*, 2016; Ransohoff, 2016)). OPC: oligodendrocyte precursor cell. NPC: neuronal precursor cell. NFT: neurofibrillary tangle.

Part 2: Aim of the Research

Dementia is a chronic and progressive syndrome associated with deficits in cognitive function. Over 50 million people world-wide have dementia (www.who.int, 12 December 2017) and, as this number keeps increasing, the associated worldwide economic burden is enormous. The high number of dementia patients and incredibly high costs for care both form the ultimate rationale to continue research on dementias in the search for a cure. Up until today, there is no such cure that can alter or reverse the disease progression, and this is mainly due to the lack of knowledge concerning the cause and disease progression mechanisms. The most studied dementia type is Alzheimer's disease (AD), most known for the presence of extracellular amyloid-beta plaques and neurofibrillary tangles (NFTs). NFTs are intraneuronal aggregates of hyperphosphorylated tau protein, which ultimately result in neurodegeneration, a process termed "tauopathy". Interestingly, in AD patients, the spread of tau aggregates, rather than the spread of amyloid-beta plaques, correlates with the clinical manifestations, indicating tauopathy is of major importance in neurodegenerative diseases and a potential therapeutic target (Riley *et al*, 2002). Recently, mutations in the MAPT (Tau) gene were identified in patients suffering from hereditary forms of Frontotemporal dementia (FTD), indicating that Tau dysfunction alone can result in neurodegeneration and dementias (Poorkaj *et al*, 1998; Hutton *et al*, 1998; Spillantini *et al*, 1998). Mouse models expressing these human mutant tau genes also show age-associated NFT formation, in complete absence of any amyloid plaques. An example is the Thy1-hTau.P301S mouse model showing neuron-specific expression of human tau with the P301S mutation (Allen *et al*, 2002). Such mouse tauopathy models can be used to unravel the mechanisms of tauopathy and investigate the role of other cells (like microglia and astrocytes) in this process, without biases induced by amyloid-beta pathology. The Elga De Vries group (which is part of the MCBI-Amsterdam UMC) has expertise in neuroimmunology and recent work (van Olst *et al*, 2018) on microglial changes in aging raised interest in the role of microglia in neurodegenerative contexts.

Microglia are the brain-resident immune cells that scan their environment and phagocytose pathogens and debris. When microglia respond to different insults, they can adapt new functions and shapes (Rock *et al*, 2004). Currently-used read-outs to study microglia are their morphology and marker-expression (e.g. MHC). The response of microglia towards tau tangles is not completely understood. Several groups have reported microglia to be in close contact with NFTs in AD brain tissue (Cras *et al*, 1991; Streit *et al*, 2009) and, due to the phagocytic nature of microglia, researchers have hypothesized microglia are able to phagocytose tangles. This idea was already supported by *in vitro* and *ex vivo* tau phagocytosis experiments (Luo *et al*, 2015) and experiments on human isolated tau species injected in the mouse brain (Bolós *et al*, 2015). *In vivo* experiments on microglial phagocytosis of tau in the demented brain of mouse tauopathy models are missing. We hypothesize microglia show an altered morphology in the brain of mouse tauopathy models (e.g. Thy1-hTau.P301S mice), and are able to internalize phosphorylated tau species expressed by resident neurons. Currently, the timing of microglial activation in response to NFTs is unclear. For example, microglial activation was observed before the onset of NFTs in a mouse model of tauopathy (Yoshiyama *et al*, 2007). The mice used in this study, however, expressed mutant tau in all brain cells, which implicates microglial activation may have occurred as a result of different mutant tau sources. Contrarily, the tauopathy mouse model created by Allen *et al,* expresses the same human mutant tau from the neuron-specific Thy1 promoter (Allen *et al*, 2002). As

such, we hypothesize that, in the Thy1-hTau.P301S mice, microglia are able to (indirectly) respond to neuronal tau expression or aggregation, and thus microglial activation occurs only after neuronal human mutant tau expression or NFT formation.

During this master dissertation, I aim at visualizing microglial morphology and correlate these with different NFT-loads. First, we need to optimize immunohistochemical (IHC) stainings that allow visualization of microglia (Iba1) and phosphorylated tau (AT8) in brain sections of non-transgenic and Thy1-hTau.P301S mice. Once optimized, we will perform these IHC stainings on sagittal sections and analyze the spatio-temporal profile of hTau expression with a standard fluorescent microscope. Interesting regions showing a gradual increase in NFT load will be analyzed extensively for microglial morphology through confocal microscopy. We aim to describe the temporal profile of region-specific microglial morphology using quantifiable measurements as surface area-, volumetric- and sholl-analysis. At this stage, we will examine when microglial morphology changes occur and investigate potential (phagocytic) interactions with NFTs. Next, we will attempt to combine an additional marker for CD68 (a lysosomal/endosomal-associated membrane protein) with the existing IHC staining protocol. Once optimized and stained, we will perform a temporal analysis of CD68 expression (surface area and volumetric) indirectly indicative for phagocytic activity. Additionally, we will investigate the lysosomal content for presence of phosphorylated tau. In conclusion, we aim to perform a spatio-temporal analysis of microglial morphology in a mouse model for tauopathy, and investigate microglial phagocytic activity and potential interactions with NFTs. In follow-up studies, the hosting group will use the optimized approach to analyze microglial morphology in Thy1-hTau.P301S mice treated with various therapeutic molecules.

Part 3: Results

The Thy1-hTau.P301S (CBA.C57BL/6) mice express human tau with a P301S mutation from the neuron-specific Thy1 promotor. To investigate the role of microglia in this mouse model of tauopathy, we optimized AT8/Iba1/CD68 immunohistochemical (IHC) stainings in brain slices of non-transgenic and Thy1-hTau.P301S animals of different ages. Images generated through confocal imaging were analyzed extensively. We investigated the 1) spatio-temporal expression of phospho tau, 2) microglial morphology, 3) temporal expression of phospho tau/Iba1/CD68, 4) microglial ramification complexity and 5) lysosomal volume and content.

3.1. Spatio-temporal expression of phosphorylated tau

To evaluate the spatio-temporal expression of phospho Tau in our cohort Thy1-hTau.P301S transgenic (hereafter P301S) mice and age-matched (2-6 months old) non-transgenic (hereafter non-tg) mice, sagittal brain sections were immunostained with the AT8-antibody (targeted against phosphorylated tau). In P301S mice, a thresholded AT8-positive surface area signal quantification in different brain regions revealed consistent signals in frontal and temporal lobes from 4 months on and robust and significant signals from 5.5 months onwards compared to 2 months old P301S animals (Figure 5). AT8-positive signals were weak in hippocampal regions. The rate at which additional neuron-like structures display phospho tau expression was region-dependent. In comparison, the cortex (and other regions, data not shown) of non-tg animals showed almost no phospho tau expression for the different time-points investigated.

3.2. Microglial morphology

To assess cortical microglial morphology, we optimized an IHC staining on sagittal brain sections (of 5.5 months old non-tg and P301S animals) visualizing microglia using Iba1 (red), phospho Tau using AT8 (green) and lysosomes using CD68 (white) expression (Figure 6). Both the anti-Iba1, anti-CD68 and their secondary antibodies stained their respective targets specifically (as shown by negative controls omitting the primary antibodies, addendum Figure 15 C and D, whereas the secondary antibody targeted against the anti-AT8 antibody showed cross-reactivity with blood vessel-resident antigens (Figure 5 and 7C, Addendum Figure 15 D and Figure 6). Noteworthy, the anti-AT8 antibody was unable to completely penetrate the tissue sections and therefore no phospho tau signals were detected in the center (in depth) of any tissue section (Addendum Figure 16). As such, about 60% of the tissue sections volume did not show any AT8 signals. Additionally, only mild autofluorescence was detected in all sections (Addendum Figure 15 A and B). As expected, almost no AT8-positive signal was detected in tissue sections of non-tg animals (that is, besides aspecific staining of blood vessels), whereas strong AT8-positive signals were visible in the soma of neurons (circle shapes) in sections of 5.5 months old P301S animals. Sections of non-tg animals showed microglia with a more ramified morphology. Sections of P301S animals showed a more heterogenic population of microglia; some characterized by a normal-looking ramified morphology, whereas others showed mild hypertrophy and a bigger soma, reminiscent of microgliosis. In sections of P301S animals, most microglia had processes extending in all directions. Processes directed against tau-positive neurons made contact with the neuronal surface. These contacts were also observed with ghost tangles (lacking a DAPI-positive nucleus and showing a more diffuse and weak AT8 signal). No clear examples were found of microglia engulfing complete neuronal somas. CD68 signals were found mostly inside Iba1-

positive cells, more specifically, in the rim of somas and processes. No clear difference in CD68 signal could be observed between non-tg and P301S animals.

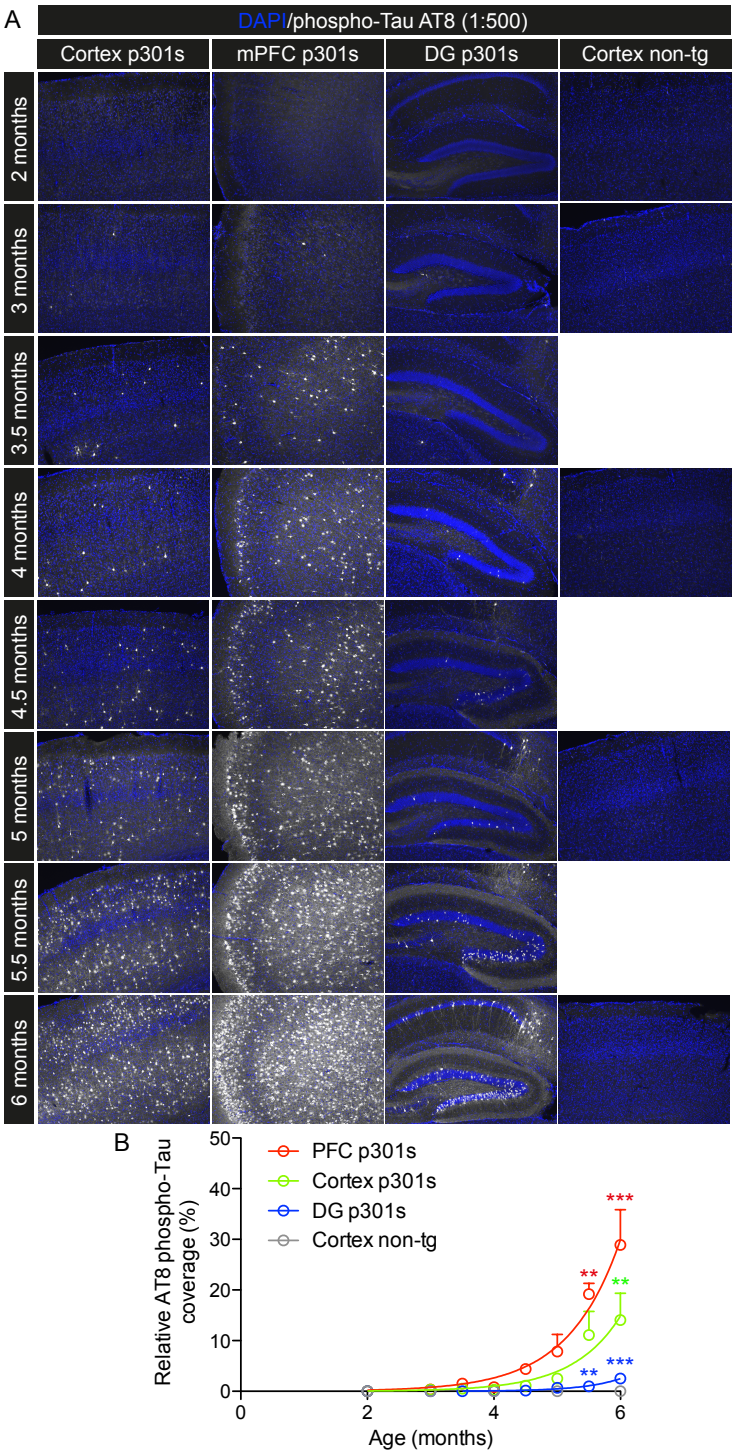


Figure 5. Spatio-temporal analysis of phospho Tau expression in different brain regions of P301S and non-tg mice. A) Representative photomicrographs depicting immunohistochemical staining for phospho tau (white) and DAPI (blue) in specific regions of sagittal brains sections of Thy1-hTau.P301S and non-transgenic mice, at different ages. Images were created through standard fluorescent microscopy, 10x magnification. B) Quantified phospho tau expression in specific regions at different ages, shown as relative surface area coverage of the total image. N≥3 in each age group. Per region, the average surface area coverage in an age group was compared to the average of 2 months old animals (One-way Anova with post-hoc Tukeys multiple comparison test). mPFC: medial prefrontal cortex. DG: dentate gyrus. * (P<0.05), ** (P<0.01), *** (P<0.001).

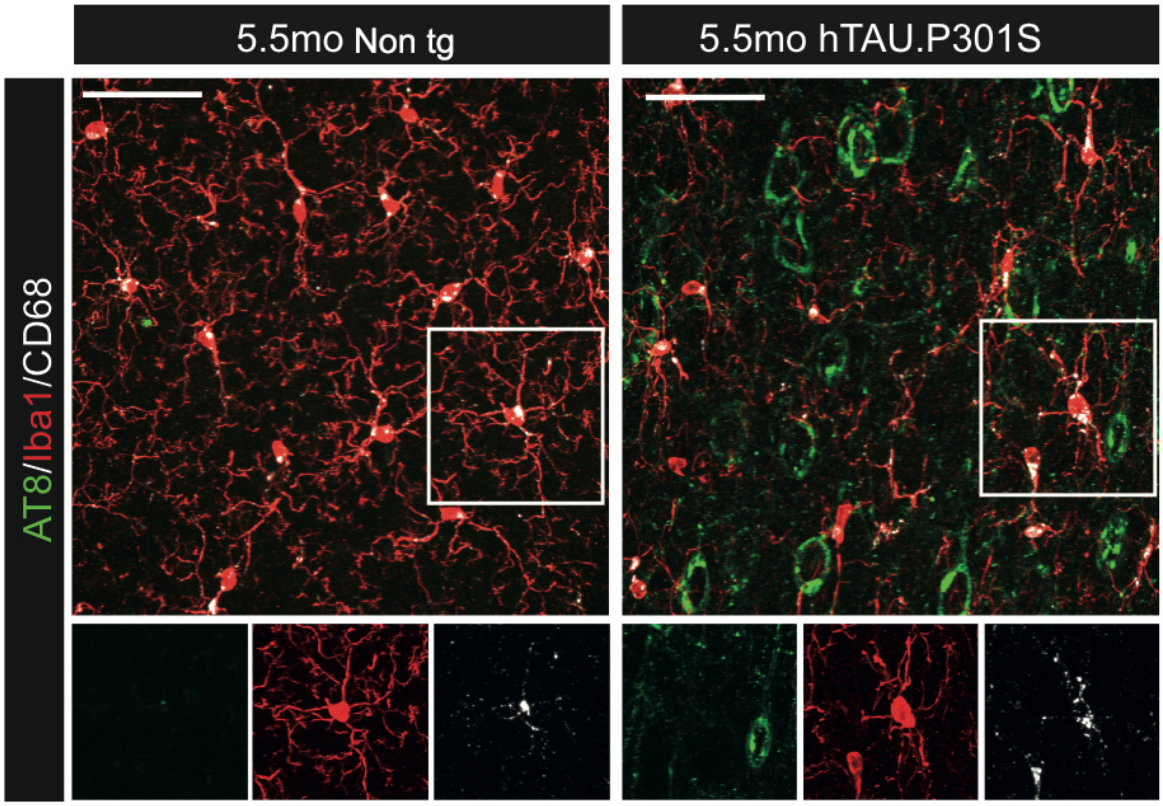


Figure 6. P301S neuroimmune profiling approach. Representative photomicrographs depicting immunohistochemical Iba1/AT8/CD68 staining of cortical regions in sagittal brain sections of Thy1-hTau.P301S and non-transgenic mice. Shown are the merge of the complete image and individual channels around a single zoomed-in representative microglial cell. Images were created through confocal microscopy, focused on cortical regions directly above the dentate gyrus (60X magnification, scale bar indicates 20 µm). mo: months old.

3.3. Temporal expression of phospho tau, Iba1 and CD68

In order to evaluate the temporal profile of phospho tau expression in relation to the microglial morphology and early endosomes/lysosomal signals, we performed the optimized IHC AT8/Iba1/CD68 staining on tissue sections of non-tg and P301S animals of different ages. We then quantified AT8/Iba1/CD68 signals as relative surface area coverage in each image (Figure 7). The temporal development of phospho tau expression imaged through confocal microscopy (Figure 7C) showed a more detailed, but highly similar overview as imaged through standard fluorescent microscopy (Figure 5 and 7A). Again, phospho tau was consistently expressed from 4 months on and strong phospho tau expression was visible in the soma of neurons (circle shapes) in sections of 5.5 months old P301S animals. Images created through standard fluorescent- or confocal microscopy showed a highly similar trend in relative AT8 phospho tau coverage. Next, in a primary attempt to quantify the temporal alterations of microglial morphology, we measured a thresholded relative Iba1 coverage per image (Figure 7E and F). Microglial number was not changed (Figure 8B) and as such discarded as a factor influencing surface area/coverage. For both non-tg and P301S animals, there was an up-and-down trend in younger animals. From 4 months of age onwards, Iba1 surface coverage was decreased in P301S animals in opposite trend of the increase in AT8 coverage. In non-tg animals, Iba1 coverage increased with age. Subsequently, we investigated the temporal changes in CD68 signals (Figure 7G and H). Unexpectedly, relative CD68 coverage was significantly higher in non-tg animals at 1 and 2 months of age, followed by a gradual

decrease until 6 months of age. Contrarily, in P301S animals, CD68 signals showed an up-and-down trend but remained (non-significantly) higher at 5 and 6 months of age.

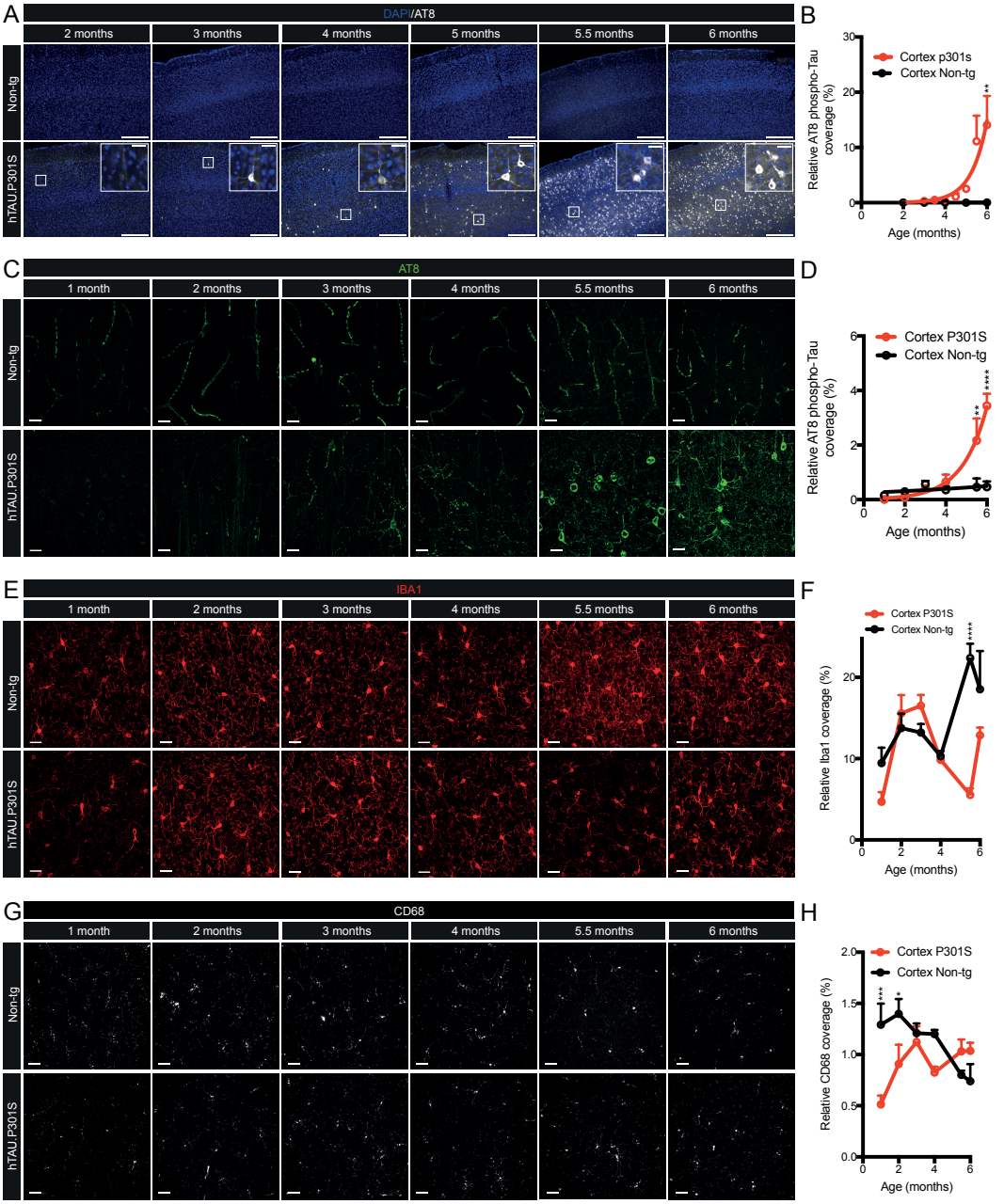


Figure 7. Temporal analysis of cortical phospho tau, Iba1 and CD68 expression. All images depict immunohistochemical stainings of sagittal brain sections of non-tg and P301S mice of different ages, focused on cortical regions. Images depicted in A) were generated through standard fluorescent microscopy (10X magnification, large scale bars indicate 2500 µm, small scale bars indicate 20 µm), as shown in Figure 5. Images depicted in C, E and G) were generated through confocal microscopy (60X magnification, scale bars indicate 20 µm). A, C, E and G) Photomicrographs depicting the temporal alterations of cortical phospho tau (white in A, green in C), Iba1 (red) and CD68 (white) expression. B, D, H and F) Quantified cortical phospho tau, Iba1 and CD68 expression at different ages, shown as relative surface area coverage of the total image. N=5 in each age group. In D) per genotype, the average surface area coverage in an age group was compared to the average of 2 months old animals (One-way Anova with post-hoc Tukeys multiple comparison test). In F and H) the average surface area coverages of genotypes were compared per age group (Two-way Anova with post-hoc Sidaks multiple comparison test). * (P<0.05), ** (0P<0.01), *** (P<0.001), **** (P<0.0001).

The temporal analysis of microglial morphology through measuring Iba1-positive surface area coverage is hampered by its inability to use the 3D information of z-stack images. In order to get a more accurate representation of microglial morphology, we measured Iba1-positive volume, rather than surface, in confocal images of cortical regions in non-tg and P301S mice of different ages using the IMARIS software (Figure 8A). For both genotypes, microglial volumes showed an up-and-down trend in younger animals, very similar to the trend observed in surface area coverage. Interestingly, no significant difference was found between microglial volumes of non- and transgenic animals of 5.5 months old, as opposed to the significant difference in surface area coverage (Figure 7F). Importantly, this effect cannot be explained by an increase/decrease in the number of microglia per image as we did not observe a significant change in microglial count between non-tg and P301S animals at any age (Figure 8B). However, for non-transgenic animals, we observed a slight (non-significant) decrease in microglial count over time, whereas in transgenic animals we observed a small (non-significant) increase.

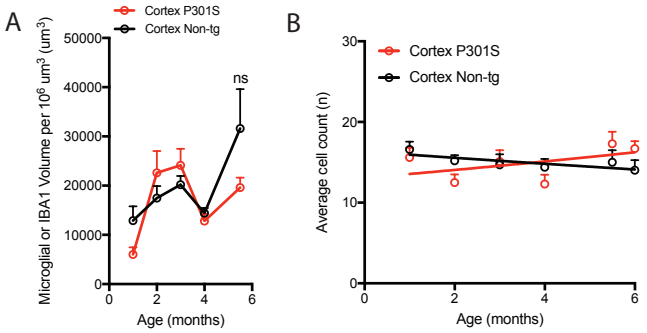


Figure 8. Temporal analysis of microglial volume in cortical regions. A) graph representing the microglial (Iba1-positive) volume in cortical brain sections of non-transgenic and Thy1-hTau.P301S mice of different age. Volumes were normalized and shown per 10^6 µm^3 volume imaged. N=5 per age and genotype. The average microglial volumes of both genotypes were compared age-by-age (Two-way Anova with Sidak's multiple comparison test). B) Best-fitting line graph representing the manual count of microglial cells per image of cortical brain regions. N=5 per age and genotype. Average cell counts of both genotypes were compared age-by-age (Two-way Anova with Sidaks multiple comparison test).

3.4. Microglial ramification complexity

To evaluate the morphology of microglial processes without any soma- or process thickness-induced biases, we performed the sholl analysis to measure microglial ramification complexity in brain sections of non-tg and P301S mice, focusing on both cortical and hippocampal brain regions (Figure 9 and 10, respectively). For this analysis, Iba1 channels of confocal images were used to manually draw microglial processes per cell. From the microglial soma center on, circles are drawn every 1 µm and the sholl software then counts the number of intersections (or microglial processes) it finds per circle. The resulting number of intersections at specific distances of the soma center are a measure of microglial ramification complexity. In cortical regions, the ramification complexity of microglia showed a decreasing trend with increasing age, but this reduction was not significant. Interestingly, ramification complexity in cortical regions of 5.5 months old P301S animals was significantly lower compared to their non-transgenic counterparts, suggesting a genotype effect in older animals but not in younger animals. On the contrary, we did not observe a significant difference in ramification complexity of microglia in hippocampal (dentate gyrus) regions of non-tg versus P301S mice (of 5.5 months old, Figure 10).

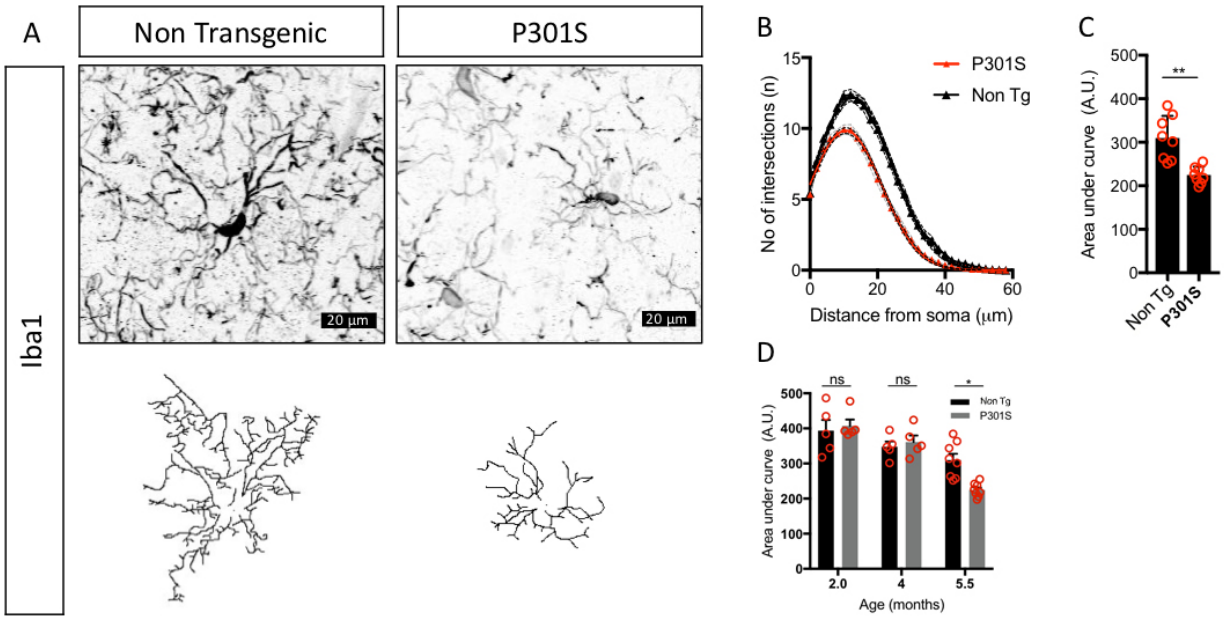


Figure 9. Temporal analysis of cortical microglial ramification complexity. A) Photomicrographs depicting representative microglia in cortical regions of sagittal brain sections of 5.5 months old non-tg and P301S mice, immunohistochemically stained for Iba1 and visualized through confocal microscopy. Ramifications were manually traced using the Fiji software and the soma center is indicated with a small dot. B) Sholl analysis was performed (using Fiji) on individually traced microglia and resulting number of intersections at specific distance from soma is plotted. C) Area under the curve was calculated for both the non-tg and P301S animals of 5.5 months old and compared through student's t-test. D) The complete work-flow was repeated in animals of 2 and 4 months of age and resulting AUCs are shown per age and genotype. Genotype effects were tested at the different ages (Two-way Anova with Sidaks multiple comparison test). N=5 per genotype for ages 2 and 4 months old, whereas nN=8 per genotype for age 5.5 mo. AUC: Area under the curve. No: Number of. A.U: Arbitrary units. * (P<0.05), ** (P<0.01), *** (P<0.001).

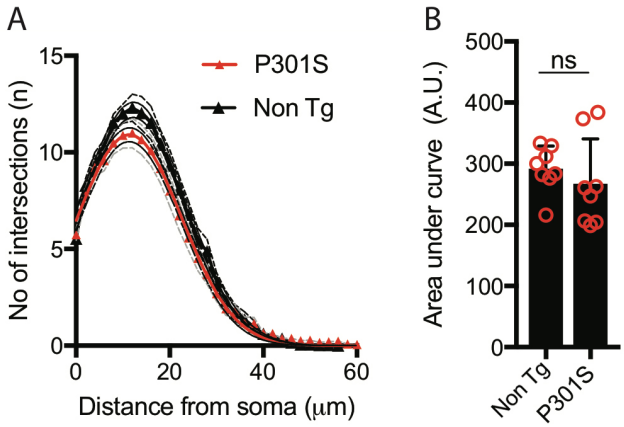


Figure 10. Analysis of hippocampal microglial ramification complexity. Sholl analysis was performed on individual microglial cells traced (using Fiji) from hippocampal (dentate gyrus) brain regions in sagittal sections of 5.5 months old and non-tg and P301S mice, immunohistochemically stained for Iba1. A) Sholl analysis was performed (using Fiji) on individually traced microglia and resulting number of intersections at specific distance from soma is plotted. B) Area under the curve was calculated for both the non-tg and P301S animals of 5.5 months old and compared through students t-test. N=8 per genotype.

The microglial ramification complexity was reduced in cortical regions of 5.5 months old P301S mice. To test if this change in morphology is dependent on the close proximity of NFTs, we performed a correlation analysis of ramification complexity in function of distance to the closest nearby AT8-positive neuronal soma (Figure 11). No significant correlation was found

(R^2=0.00175, p=0.68). Interestingly, we frequently observed a reduced ramification complexity in the microglial half facing the closest nearby AT8-positive neuronal soma. To evaluate and quantify this observation, we therefore introduced an analysis which we coined the "half sholl analysis" (Figure 12). In this analysis, all traced microglial cells were divided in two halves: an AT8-positive neuronal soma-facing side and the opposite facing side. Subsequently, we evaluated and compared ramification complexity of the different halves. As control for physiological differences in morphology due to the cortical orientation of microglia, we divided all traced cells (in cortical regions of 5.5 months old non-tg animals) in a dorsal and ventral half and again evaluated and compared ramification complexity of the different halves (Figure 12A, C and D). This revealed that the ramification complexity of ventral sides of microglia was significantly smaller compared to their dorsal counterparts. To control for this physiological difference in orientation, we removed traced cells for which the angle between microglial and AT8-positive soma was in between -45° and -135° from the dataset of 5.5 months old P301S mice, and only then evaluated and compared ramification complexity (Figure 12B, E and F). After the correction, we observed no more significant difference in ramification complexity between AT8-positive neuronal soma-facing sides and the opposite facing sides.

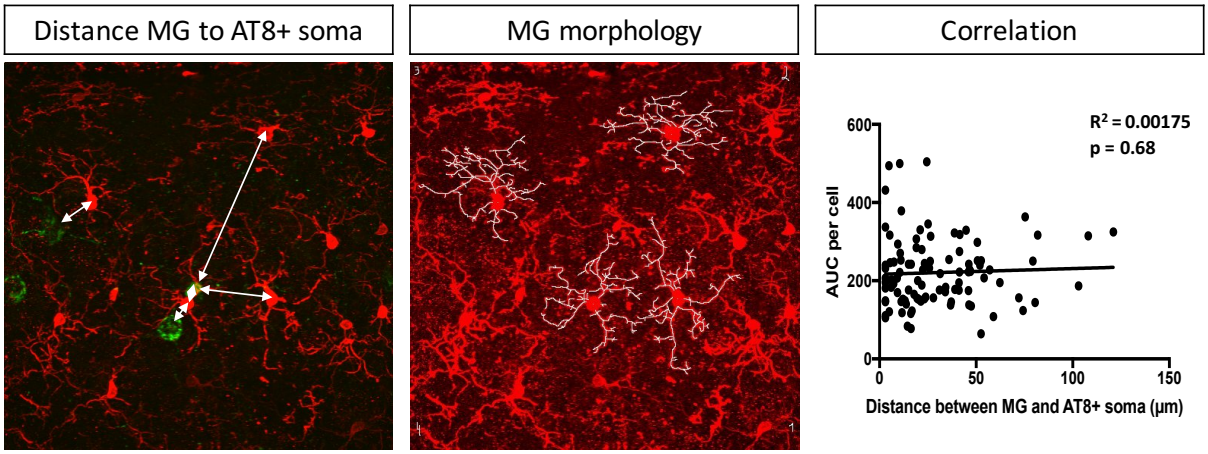


Figure 11. Correlation analysis of microglial morphology and distance to closest nearby AT8-positive neuronal soma. Representative photomicrographs depicting cortical regions in sagittal brain sections of 5.5 months old P301S mice (N=8), immunohistochemically stained for Iba1 (red) and AT8 (green). The distance between a (traced) microglia and the closest nearby AT8-positive neuronal soma was measured in z-stacked (2 Dimensional) images. Sholl analysis was performed on individually traced microglia and the number of intersections in function of distance from the soma was counted and plotted. The resulting curve was used to calculate an area under the curve value (AUC). The correlation analysis was performed using Prism7.

3.1. Lysosomal volume and content

In order to get a more accurate representation of the temporal alterations of CD68 signals, we measured CD68-positive volumes inside the iba1-positive microglia in confocal images of cortical regions of non-tg and P301S mice at different ages (Figure 13). The relative CD68 volume in microglia stayed constant in 2, 3 and 4-month-old animals, but increased in 5.5-month-old P301S animals and decreased in the non-tg mice (Figure 13F). Interestingly, this significant difference between genotypes at 5.5 months of age was not associated with a difference in lysosomal objects counted, but rather an increase in average lysosomal object volume (Figure 13C, D and E, respectively).

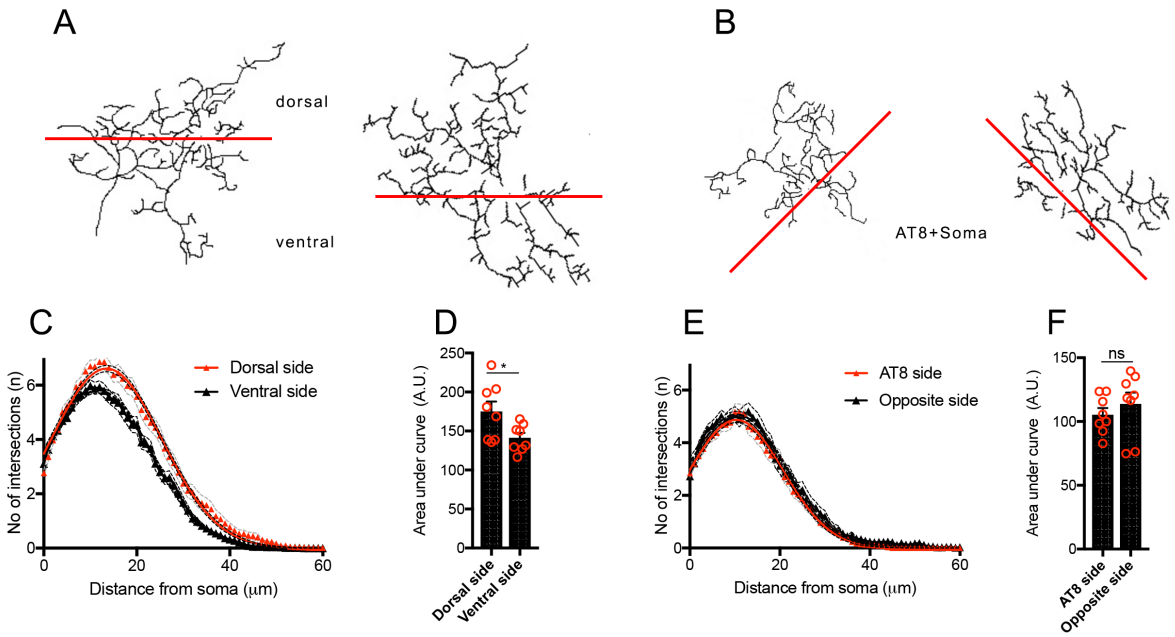


Figure 12. Half-sholl analysis of cortical microglial ramification complexity. Photomicrographs depicting traced microglia in cortical regions of sagittal brain sections of 5.5 months old non-tg and P301S mice (N=8 per genotype), immunohistochemically stained for Iba1 and visualized through confocal microscopy. Ramifications were manually traced using the Fiji software and the soma center is indicated with a small dot. A) Schematic example of how individually traced microglia, from non-tg mice, were divided in a dorsal and ventral half. B) Schematic example of how individually traced microglia, from P301S mice, were divided in an AT8-positive neuronal soma-facing side, and the opposite facing side. C and E) Sholl analysis was performed (per traced cell, using Fiji) and the number of intersections in function of distance from the soma was platted. D and F) Area under the curve values (AUC) were calculated for dorsal and ventral halves (for non-tg animals), and AT8-positive neuronal soma-facing side and opposite halves (for P301S mice). AUCs were compared through students t-test. No: number of. A.U: arbitrary units. * (P<0.05).

During preliminary analysis of the temporal alterations of CD68 signals inside microglia, we detected AT8 signals inside CD68 signals masked for Iba1, suggesting the presence of phosphorylated tau inside microglial lysosomes/early endosomes. To evaluate and quantify this observation, we measured AT8-positive volumes inside CD68 signals (masked for Iba1 signals) in confocal images of cortical regions in non-tg and P301S mice of different ages (Figure 14). We observed a time-dependent increase in relative AT8 volume in Iba1-positive masked lysosomes in both non-tg and P301S animals (which was significant in 5.5 months old P301S animals compared to 2 months old P301S animals). Obviously, almost no AT8 positive signals were expected in non-tg animals as these animals barely show any phospho tau expression. Upon further inspection of images of these non-tg animals, we found that nearly all AT8 signals supposedly inside microglial lysosomes were in very close contact with aspecifically stained blood vessel antigens and thus could have resulted from overlap in fluorescence signals (Data not shown). Interestingly, in P301S animals, AT8 signals were most frequently observed in lysosomes located rather distant from the soma and closer towards the end of ramifications (Figure 14, white arrow).

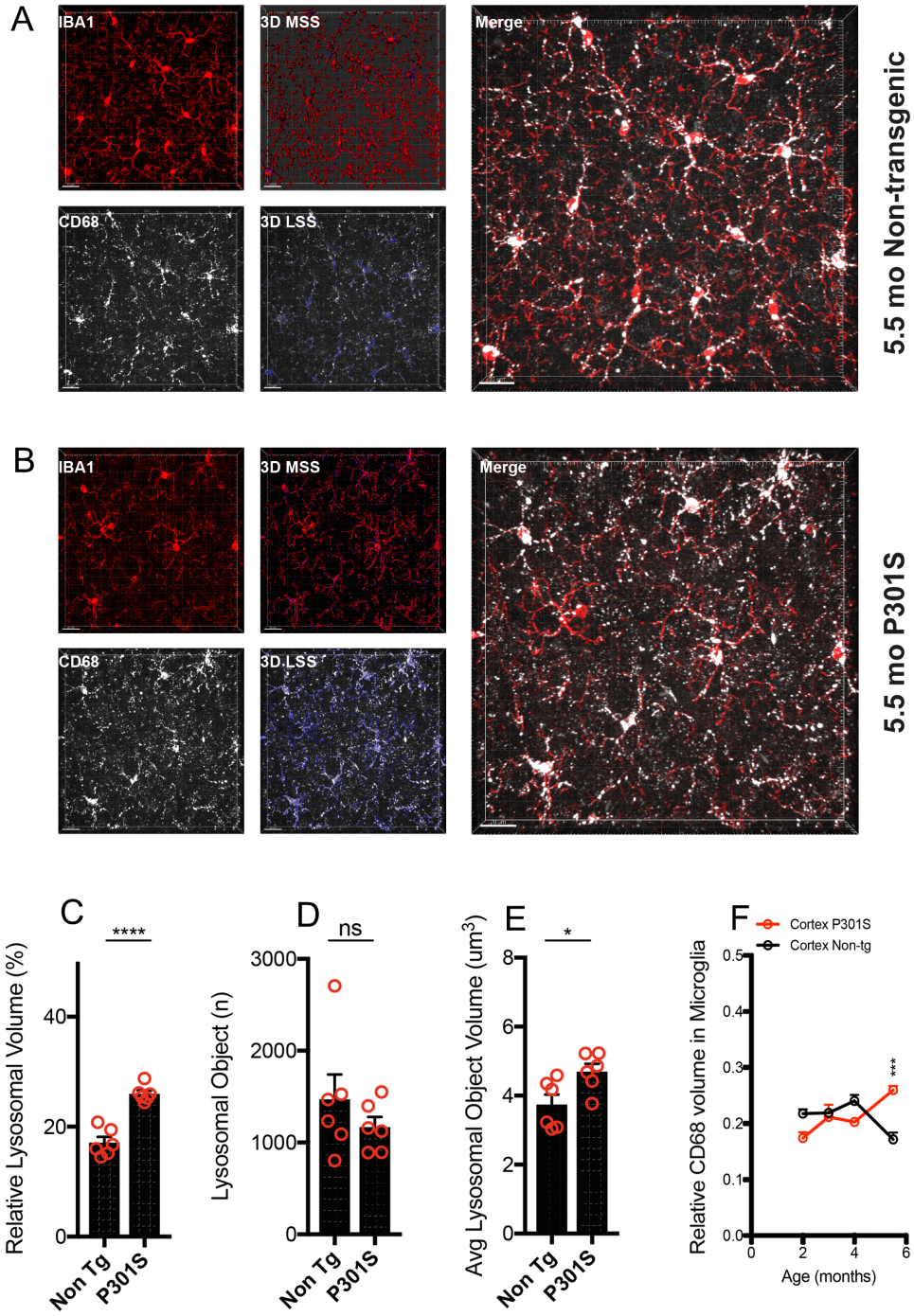


Figure 13. Temporal analysis of microglial early endosomal/lysosomal volumes in cortical regions. A and B) Representative photomicrographs depicting cortical regions in sagittal brain sections of P301S and non-tg mice of 5.5 months old (N=6 per genotype), immunohistochemically stained for Iba1 (red) and CD68 (white) and visualized through confocal microscopy and analyzed with IMARIS (scale bars indicate 20 µm). The Iba1 channel was used to create 3D microglial surface simulations (3D-MSS, shown in red). The CD68 channel was masked for the 3D-MSS and again used to create 3D lysosomal surface simulations (3D-LSS, shown in blue). C, D and E) Relative lysosomal volume, lysosomal object count and Average (Avg) lysosomal object volume were calculated and compared through student's t-test. F) The complete work-flow was repeated in animals of 2, 3 and 4 months of age (N=5 per age and genotype) and resulting relative CD68 volume inside microglia is shown per age and genotype. Genotype effects were tested at the different ages (Two-way Anova with Sidaks multiple comparison test). * (P<0.05), ** (P<0.01), *** (P<0.001), **** (P<0.0001).

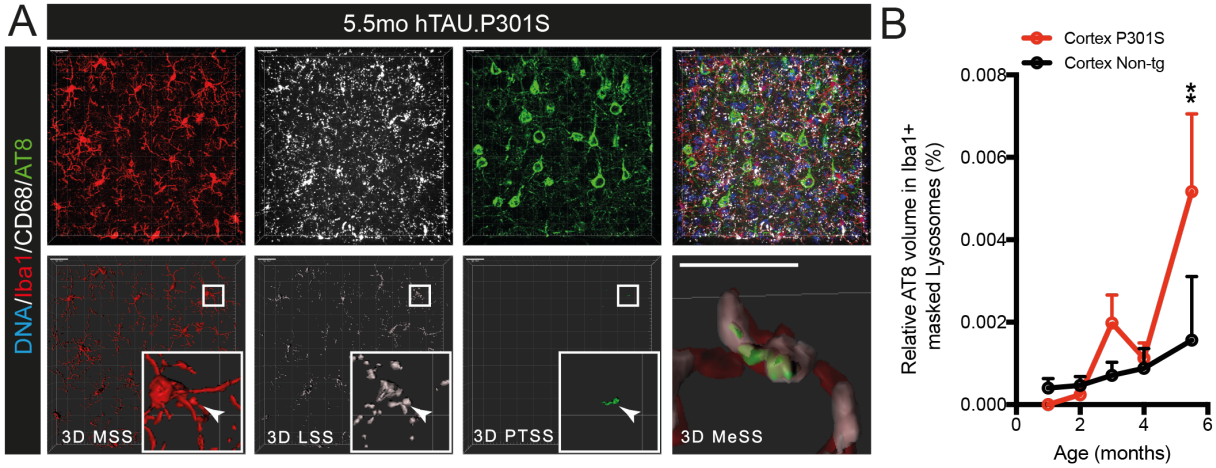


Figure 14. Temporal analysis of phospho tau content inside microglial lysosomes. A) Representative photomicrographs (top) of Iba1 (red), CD68 (white), AT8 (green) and merged channels (contains DAPI (blue) signals) of immunohistochemically stained cortical brain regions of 5.5 months old P301S mice, imaged through confocal microscopy. Individual channels were used to create surface simulations (bottom) using IMARIS. The Iba1 channel was used to create 3D microglial surface simulations (3D MSS, shown in red). The CD68 channel was masked for the 3D MSS and again used to create 3D lysosomal surface simulations (3D LSS, shown in white). AT8 channel was masked for the 3D-LSS and again used to create 3D phospho tau surface simulations (3D PTSS, shown in green). Merge of all surface simulations (3D MeSS) is shown on the bottom right. White arrows indicate the exact same location within the z-stack image. Scale bars indicate 20 µm. B) Relative AT8 volume in Iba1-positive masked CD68 signals was calculated with IMARIS. Per genotype, the average AT8 content in an age group was compared to the average of 2 months old animals (One-way Anova with post-hoc Tukeys multiple comparison test). N=5 per age and genotype. * (P<0.05), ** (P<0.01).

Part 4: Discussion

The role of microglia in tauopathies, and more specifically the response of microglia towards phosphorylated tau, is incompletely understood. The close contact of microglia and NFTs, and the phagocytic nature of microglia have led researchers to hypothesize that microglia are able to phagocytose tangles, which was also supported by *in vitro* and *ex vivo* tau phagocytosis experiments using healthy microglia (Luo *et al*, 2015; Bolós *et al*, 2015). However, no reports were made on *in vivo* experiments of tau phagocytosis by microglia present in the demented brain. We hypothesized microglia to show an altered morphology in the brain of mouse tauopathy models (e.g. Thy1-hTau.P301S mice), and are able to internalize phosphorylated tau species expressed by resident neurons. Furthermore, the timing of microglial activation and/or phagocytosis in mouse tauopathy models is unclear. As such, we hypothesized that, in the Thy1-hTau.P301S mice, microglia are able to (indirectly) respond to neuronal phospho tau expression or aggregation, and thus microglial activation occurs only after neuronal human mutant tau expression or NFT formation.

We evaluated the spatio-temporal expression of phospho tau in sagittal brain sections. For the different regions investigated in P301S mice, we found phospho tau was consistently expressed from 4 months on and this was significant from 5.5 months on. On the contrary, almost no phospho tau expression was observed in non-tg animals. For the different regions investigated, cortical regions showed the most consistent and gradual increase in phospho tau expression. Additionally, tauopathy-induced neurodegeneration has already been described in the cortex of P301S animals, suggesting microglial activation in cortical regions would be obvious and easy to detect (Allen *et al*, 2002). Therefore, for most upcoming experiments, we focused on cortical regions. In cortical regions of 5.5 months old P301S animals, which are characterized by strong phospho tau expression in neurons reminiscent of NFTs, we observed a morphologically heterogenic population of microglia. More specifically, most microglia showed mild hypertrophy and a bigger soma, reminiscent of microgliosis, whereas some showed a more ramified morphology. Other groups have also reported on the heterogeneity of microglial populations, ranging from different morphologies to different transcriptomic profiles in both health, aging and disease (Galatro *et al*, 2017; Grabert *et al*, 2016). Interestingly, we observed frequent interactions between microglial end processes and the surface of phospho tau expressing neurons. No examples were found of microglial cells engulfing complete neurons. Even though such phagocytosis events are transient processes and therefore might be hard to visualize in single stainings, the large number of analyzed images empower the validity of our observations.

To quantify these apparent microglial morphological differences at different time points, we evaluated Iba1 surface area coverage-, volumetric- and sholl analyses. Both the Iba1 surface area coverage and volumetric analyses showed an up-and-down trend in younger animals of both genotypes. Differences between genotypes were only apparent at 5.5 months of age, suggesting specific events at 4 months mark the origin of a different microglial morphological response in non-tg versus P301S mice. Interestingly, this time point coincides with consistent phospho tau expression, the relevance of which is discussed below. As we expected microglial ramification complexity to decrease in P301S animals, we also expected the Iba1 surface area coverage to decrease with time. However, our results did not show such a clear decreasing trend. Notably, our current analysis does suffer from several technical limitations. For example, the total Iba1 surface area coverage is a result of signals from microglial soma and

processes. As microglial activation imposes the enlargement of soma (also called amoebification) and thicker but more retracted processes, any change in total Iba1 surface coverage is difficult to assign to soma or processes (van Olst *et al*, 2018; Fernández-Arjona *et al*, 2017). In that sense, measuring these structures individually should give more accurate results. For example, measuring soma surface/volume alone would be more meaningful to investigate amoebification, whereas the sholl analysis (see further) can single out the influence of retracted/shorter processes or a reduced ramification complexity. Altogether, the Iba1 surface coverage- and volumetric analysis did not allow us to clearly quantify the earlier observed change in microglial morphology in P301S mice compared to non-tg mice. Noteworthy, observed changes in Iba1 surface or volume could not be explained by a change in number of microglia as only very slight changes were observed. The slight decrease in microglial count observed in non-tg animals is contradicting earlier reports stating the number of microglia increases with age as individual microglia become less capable (Long *et al*, 1998; Vaughan & Peters, 1974; Tremblay *et al*, 2012). However, the animals used in our study are relatively young and only cortical microglia were imaged, compared to the rather old microglia in hippocampal, visual, auditory and retinal regions investigated by these groups. Our findings are, however, in line with reports of other groups stating the number of microglia remains relatively constant throughout life and even after early life insults (Bland *et al*, 2010; Williamson *et al*, 2011). Investigating such microglial proliferation as a result of NFT onset in older animals would be interesting. However, as most P301S animals die before the age of 8 months (www.alzforum.org, Thy1.P301S), this may be difficult and other mice models should be considered.

To evaluate the morphology of microglial ramification complexity without any soma- or process thickness-induced biases, we performed the sholl analysis on tracings of of Iba1 stained microglia. In cortical regions, the microglial ramification complexity decreased with age, but differences between genotypes were only apparent at 5.5 months of age. More specifically, the overall ramification complexity of 5.5 months old P301S microglia is smaller compared to age-matched non-tg microglia and, as such, confirms our hypothesis that microglial morphology is altered in P301S mice. Again, these results suggest specific events at around 4 months of age mark the origin of a different microglial morphological response in non-tg versus P301S mice. Interestingly, the changed morphology of microglial ramifications in older animals was not dependent on the close proximity of AT8-positive neuronal somas. This analysis thus suggests the distance between microglial- and AT8-positive neuronal somas is not important or, alternatively, it might point to the importance of the position/location of microglial ramifications instead of the soma. Contrarily, other groups have reported activated microglia to be closely associated with AT8-positive neuronal somas throughout the brain and spinal cord (Bellucci *et al*, 2004), but did not specifically report the distance per se. It remains to be seen at what distance microglia are still able to respond to neuronal phospho tau expression or, alternatively, respond to indirect factors released by AT8-positive neuronal somas. The current analysis does, however, suffer from several technical limitations. Firstly, the anti-AT8 antibody did not completely penetrate the tissue sections and therefore no tangles are stained in the center (in depth) of the tissue section. A large number of AT8-positive neuronal somas may therefore be missed in this analysis, resulting in an overestimation of the distance to the closest AT8-positive tangle. Simply using thinner tissue sections to solve this issue is not possible, because smaller sections (<40 µm) cannot completely contain microglial cells with their fully extended processes. Secondly, the distance

between microglial and AT8-positive neuronal somas was measured on the 2D-stacked image, resulting in an underestimation of the distance. In future analysis, measuring the distance in the 3D non-stacked image should resolve this issue. Finally, the current set-up only looked at the closest AT8-positive neuronal soma, and any additional nearby neurons were completely ignored. Altogether, our current analysis does not allow to specify a distance from which microglia change their morphology as response to the presence of NFTs, but did clearly show that microglial ramification complexity is reduced only after NFT onset.

During the sholl analysis, we made the preliminary observation that ramifications facing AT8-positive neuronal somas looked less complex. To this end, we introduced the "half sholl analysis", which measures the ramification complexity of 2 halves of each cell. To control for physiological differences in morphology due to the cortical orientation of microglia, we evaluated dorsal and ventral ramification complexity of traced cells. Unexpectedly, ventral sides of microglia showed a reduced ramification complexity compared to the dorsal halves. These results can be explained by the physiology of the imaged regions. More specifically, we imaged microglia residing in cortical layer II and on the border of layer I and II. No neuronal somas are present in cortical layer I (Gilmore & Herrup, 1997) and, as such, microglia have more free space to extend their processes in dorsal directions. On the contrary, cortical layer II is packed with neuronal somas and therefore microglia have less free space to project processes ventrally. When correcting for this physiological difference in microglial ramification complexity, we did not observe a significant complexity difference anymore between the AT8-facing halves and opposite facing halves in 5.5 months old P301S animals. However, once again this analysis is biased by the uncertainty if the chosen AT8-positive soma is actually the closest one, because the distance was measured on the 2D-stacked image and no AT8 signals were observed in the center (in depth) of the tissue section. Nonetheless, using the half sholl analysis we were unable to confirm our earlier observations and conclude microglial ramification complexity is not specifically altered towards the closest AT8-positive neuronal soma.

Interestingly, no microglial ramification complexity differences were observed in the hippocampus of non-tg and P301S animals of 5.5 months old. The development of tauopathy in hippocampal regions was already shown to proceed at a slower pace compared to other regions (Snowden *et al*, 2002) in human FTD patients. Although it is difficult to compare these findings with the tauopathy development in mice, it could mean that 5.5 months is "too young" to observe a changed morphology of microglial ramifications. These reports are further supported by our observations of rather low phosphorylated tau signals in hippocampal regions of 5.5 months old P301S animals. Additionally, Grabert *et al* have also shown that microglia in the hippocampus of young animals are more immune vigilant compared to cortical microglia (Grabert *et al*, 2016). As we hypothesized microglia to respond to the onset of NFTs or phospho tau by changing their morphology, we hereby support this hypothesis by showing microglia do not show a changed morphology in regions where no NFTs are present and/or phopsho tau expression is very low. Our data do, however, contradict some of the observations of Belluci *et al*, who reported on activated microglial cells throughout the brain and in the hippocampus of 5 months old P301S mice, opposed to ramified microglia in the brains of control mice (Bellucci *et al*, 2004). Noteworthy, the group did not quantify any of the proposed microglial morphologies nor did they mention the number of animals/tissue sections/images used, again indicating that quantifying

morphological changes and giving all technical details is of major importance to allow comparing inter-experimental differences. As an example, for 5.5 months old non-tg and P301S animals, we found peak values of 12 and 10 intersections around 15 µm radius away from the soma, respectively. In comparison, Van Olst *et al* used the sholl analysis to evaluate ramification complexity of 6 months old non-tg animals, and found peak values of only 7 intersections around 15 µm radius away from the soma (van Olst *et al*, 2018). However, they performed the sholl analysis on images generated through standard fluorescent microscopy and might have missed many branches only visible through e.g. confocal imaging. Our data therefore suggest high resolution imaging can be an added value when performing the sholl analysis, and accounting for the imaging technique used is important to evaluate inter-experimental differences. Comparing sholl analysis results of cortical microglia was not possible, because, to our knowledge, no groups have used the sholl analysis to evaluate cortical microglial ramification complexity.

Besides a changed microglial morphology, we hypothesized microglia would be able to internalize phosphorylated tau species expressed by resident neurons. To evaluate microglial phagocytosis, we investigated the temporal profile of early endosomes/lysosomes (which are indirect markers for phagocytic activity) through CD68 IHC stainings of brain sections of non-tg and P301S mice of different ages. To quantify CD68 signals, we measured a thresholded CD68 surface area coverage and volumes inside tissue sections. Unexpectedly, relative CD68 coverage was significantly higher in non-tg animals at 1 and 2 months of age, compared to age-matched P301S mice. Contrarily, in P301S mice, CD68 signals showed an up-and-down trend but remained (non-significantly) higher at 5 and 6 months of age, compared to age-matched non-tg mice. Notably, in the current analysis we did not mask CD68 signals towards Iba1 signals, indicating the measured CD68 surface area coverage results from microglial and other sources combined. Other groups have shown CD68 signals to be present in astrocytic lysosomes, ghost tangles, senile plaques and perivascular deposits, which could bias our current analysis (Kobayashi *et al*, 1998, 2002). Fortunately, senile plaques are only present in older animals, and should therefore not influence the current analysis. Nonetheless, as we cannot be sure of the contribution of microglial CD68 signals, it is hard to draw conclusions based on the CD68 surface area coverage analysis. Additionally, measuring CD68-positive surface area coverage is inaccurate due to its inability to use the 3D information of confocal z-stack images. As a solution, we measured relative CD68 volumes (masked for microglial/Iba1 signals) instead of surface area coverage. The relative CD68 volume in microglia remained constant in 2, 3 and 4-month-old non-tg and P301S animals, but increased in 5.5-month-old P301S animals and decreased in the non-tg mice. Again, specific events at around 4 months of age mark the origin of a different microglial response, now present as an increase in relative lysosomal volume. Noteworthy, AM Wong *et al* observed an age dependent increase in CD68 expression in multiple brain regions, suggesting the CD68 increase we observed may be biased by aging (Wong *et al*, 2005). However, the group only investigated CD68 expression in non-transgenic animals of either 4 or 24 months of age, suggesting the rather young age of animals included in our analysis should not be biased by true aging effects, but represents a differential response of microglia towards the presence of NFTs. Additionally, our results are in accordance with earlier observations of CD68 signals in activated microglial cells nearby amyloid plaques and NFTs in mouse models for AD and even human AD brains (Bornemann *et al*, 2001; Kobayashi *et al*, 1998; Sasaki *et al*, 2002). Interestingly, the observed significant difference in lysosomal volume between genotypes at

5.5 months of age is not associated with a difference in lysosomal objects counted, but rather an increase in average lysosomal object volume. These data suggest no net increase in lysosomes, but already-present lysosomes become bigger, potentially through uptake of internalized debris. More proof-of-concept research is needed to confirm this hypothesis. Additionally, repeating our experiments with a different marker for lysosomes (e.g. lysosomal-associated membrane protein 1 (LAMP1)) would be interesting, because the lysosome-specificity of CD68 is still under debate (Kobayashi *et al*, 1998, 2002). Altogether, the observed increase in CD68 signals in older P301S mice is an indirect marker for increased phagocytic activity which only occurs after NFT onset or consistent phospho tau expression.

Subsequently, we checked the lysosomal volumes for the presence of AT8 signals. Until now, only few groups have described tau phagocytosis by microglia. Firstly, proof-of-concept for microglia phagocytosing tau species was provided by Luo *et al*, who showed that mouse microglia can internalize and degrade hyperphosphorylated pathological tau species (isolated from human AD brains) *in vitro* (Luo *et al*, 2015). The same microglia were also able to degrade free tau species released from brain tissue sections of Thy1-hTau.P301S mice. Similar observations were made by this group when human brain tissue sections were used. Secondly, Bolos *et al* reported that healthy mouse microglia can phagocytose tau isolated from AD brains and injected in the mouse brain (Bolós *et al*, 2015). Additional *in vivo* phagocytosis observations were also reported in marmosets, a non-human primate (Rodriguez-Callejas *et al*, 2016). The reports of Luo and Bolos *et al*, however, only described tau phagocytosis by healthy microglia, not confronted with a neurodegenerative environment. To date, no groups have reported on (*in vivo*) tau phagocytosis of microglia present in the demented brain. In our current study, we observed a time-dependent increase in relative AT8 volume in Iba1-positive masked lysosomes in cortical regions of both non-tg and P301S animals. Obviously, almost no AT8 positive signals were expected in non-tg animals as these animals barely showed any phospho tau expression. Upon further inspection of these non-tg animals, we found that nearly all AT8 signals supposedly inside microglial lysosomes were in very close contact with aspecifically stained blood vessel antigens and thus could have resulted from overlap in fluorescence signals. In order to ensure the detected AT8 signals inside lysosomes are not a result of fluorescence overlap, we should deconvolute images or, ideally, explore 3D-SEM (3-dimensional scanning electron microscopy) as an imaging approach with an even higher resolution. Alternatively, perivascular macrophages (which are also stained by Iba1) could also have internalized blood-resident IgG molecules which were bound to the secondary anti-mouse antibody used to detect the primary mouse anti-AT8 antibody. The presence residual mouse IgG molecules can be avoided by performing a more optimal perfusion, removing as much blood as possible from the vasculature. Alternatively, mouse-on-mouse antibody detection kits can be used to avoid this problem. Fortunately, several images from non-tg animals did not show any blood vessels present and did not show any AT8 signals inside any of the microglia, supporting the idea that nearly all detected AT8 signals inside non-tg lysosomes are a result of aspecific antibody binding. As stated earlier, we also observed a time-dependent increase in relative AT8 signal inside P301S microglial lysosomes. Notably, only very low amounts of AT8 signals were detected inside the microglial lysosomes, but we expect this to be an underestimation since the AT8 antibody was not able to completely penetrate the tissue sections. Interestingly, in these P301S microglia, AT8 signals were most frequently observed in endo-/lysosomes located rather distant from the soma and closer towards the end of ramifications. This is the location of intracellular vesicles

which were recently created through e.g. phagocytosis or pruning synapses at the very end of microglial processes. In such “early” lysosomes, the pH is still neutral and thus, after penetration, the anti AT8 antibody can still bind to the target phosphorylated tau molecules. Contrarily, “late” lysosomes are characterized by a lower pH, which activates resident phosphatases targeting tau molecules (Godbey, 2014). As a result, the anti AT8 antibody would not be able to recognize unphosphorylated tau species present in late lysosomes. It would be interesting to use phosphorylation-independent tau antibodies (e.g. HT7) and evaluate if there is a shift towards lysosomes closer to the soma, supporting the idea of a transfer from e.g. synaptically pruned phosphorylated tau towards late lysosomes. Altogether, the lysosomal content analysis revealed the presence of phosphorylated tau species and thus provides evidence that microglia in the demented brain or neurodegenerative environment are in fact able to phagocytose neuronal sources of phosphorylated tau.

In the current study, we did not investigate which neuronal structure was the source of internalized phosphorylated tau. However, we did not observe microglia engulfing complete AT8-positive neuronal somas, whereas we did see microglial processes in contact with the surface of AT8-positive neurons and more diffuse-like structures reminiscent of ghost tangles. Although speculative at this point, we suggest the microglial AT8 signal within the CD68-positive volumes could originate from synaptic or ghost tangle phospho tau. For example, neuronal synapses, or more specifically, pre- and post-synaptic elements can be visualized through synaptophysin- and post synaptic density protein 95 stainings, respectively. It would be interesting to check microglia for the presence of cellular inclusions reminiscent of axon terminals or dendritic spines, an observation which was made earlier by Tremblay *et al* when looking at microglial interactions with synaptic elements in the cortex (Tremblay *et al*, 2010). If found, these structures might help explain the source of internalized phosphorylated tau in our current study. Concurrent with this idea, synapse loss and microglial activation were also observed in a mouse model for tauopathy, but the association between both was not investigated by the research group (Yoshiyama *et al*, 2007).

Research on the role of microglia in pure tauopathies is steadily increasing, but is still in its infancy. As such, most research groups are currently focusing on the most obvious way to approach a new problem: by looking at it. To this end, various imaging approaches are used to visualize various cellular and molecular targets in the brain and nervous tissue. In our current study, we show that images generated through confocal microscopy offer the possibility to investigate different AT8, Iba1 and CD68 positive structures in more detail, without compromising reproducibility of quantified data of a more zoomed-out image generated through standard fluorescent microscopy. In our study of the P301S mouse tauopathy model, we have shown that cortical P301S microglia show a reduced ramification complexity, reminiscent of an activated-like morphology, compared to old non-transgenic animals. Moreover, an increase in CD68 volume was observed suggesting P301S microglia are more phagocytic. For the first time, we here describe internalization of tau by microglia present in the demented brain of tauopathy mice. Interestingly, the morphological and phagocytic changes were only observed in 5.5-month-old animals. No differences were found between non-tg and P301S animals of 4 months old, suggesting specific events during the 4^{th} month of life mark the origin of a different microglial response. As such, the cortical microglial activation in P301S mice only occurs after consistent phospho tau expression or NFT

formation. The role of microglia in tauopathies remains unclear. Currently, researchers have hypothesized two potential roles for microglia. Firstly, tauopathy models have shown that neuroinflammation is the prime source to drive tau aggregation and finally neurodegeneration (Bellucci *et al*, 2004; Zilka *et al*, 2009). Neuroinflammation also indirectly activates microglia, and microglial activation in turn aggravates tauopathy (Maphis *et al*, 2015). If the neuronal source of internalized tau appears to be synaptic elements, this could imply that therapeutically promoting microglial phagocytosis/uptake might increase the rate of synaptic removal and therefore be even more detrimental. Notable, excessive synaptic removal was already observed in AD patients (Scheff & Price, 2006). In other words, this first view presumes microglia are detrimental and might even aid the process of NFT formation. Such microglial activation was found to occur even before onset of NFTs in the MoPrP-hTau.P301S mouse model for tauopathy (Yoshiyama *et al*, 2007). However, this study used a mouse model expressing human mutant tau from the murine prion promoter, which is active in nearly all CNS cells. Therefore, microglial activation may have resulted from either responding to neuronal, microglial or other sources of phosphorylated tau. The current study contradicts these observations, as microglial activation was only observed after onset of NFTs and thus suggesting microglia don't play a major role in NFT formation. However, our findings don't exclude the possibility that microglia can aid in the spread or propagation of phosphorylated tau species. Nonetheless, our results support the 2nd potential role attributed to microglia in tauopathy. This second view states microglia have a rather protective role through uptake of excess tau thus protecting neurons from accumulating tau species and reducing the rate at which tau spreads from neuron to neuron (Holmes *et al*, 2013, 2014). It would be interesting to check if therapeutically promoting microglial phagocytosis or internalization of phopsho tau is able to reduce NFT-induced neurodegeneration and improve behavior and survival in Thy1-hTau.P301S animals. For example, a non-selective PPAR modulator DSP-8658, was used to treat mouse models of AD and was shown to improve memory through enhanced microglial phagocytosis of amyloid-beta fragments (Yamanaka *et al*, 2012). As we did not observe engulfment of complete neurons, we hypothesize microglia take up phospho tau by internalizing ghost tangles or pruning tau-positive synapses. Future research should aim to identify the exact structural source of internalized tau. If the neuronal source of internalized tau appears to be ghost tangles, then promoting microglial phagocytosis or uptake could have beneficial effects as this would imply a more rapid and more efficient clearance of tau debris that could otherwise spread and affect nearby healthy neurons. Such mechanisms are in line with the idea that loss of microglia is a driving force in tauopathies. Additionally, the impact of tau uptake on microglial functioning is currently unknown. It is possible that tau build-up is not broken down but accumulates in microglia, suggesting microglia themselves may die as a result of excessive tau uptake. In line with this idea, Callejas *et al* observed phospho tau inside dystrophic microglia, but not in active-looking microglia in brains of old marmosets (a non-human primate) (Rodriguez-Callejas *et al*, 2016). In the current study, however, we only observed small amounts of phospho tau signals inside microglial lysosomes, suggesting tau build-up and aggregation takes a long time or, alternatively, suggesting microglia can easily cope with internalized phospho tau. Nonetheless, more research is needed to uncover the functional implications of tau uptake by microglia.

In our study of Thy1-hTau.P301S tauopathy mice, we found microglia to show a reduced ramification complexity and increased lysosomal volumes, indicative of an increased

phagocytic activity. These altered microglial responses were apparent only after consistent phospho tau expression or NFT onset. Strikingly, we observed phospho tau signals inside microglial lysosomes and thus show that microglia, present inside the demented brain, are able to internalize neuronal sources of phospho tau. We did not observe microglia engulfing complete neuronal somas and therefore, although speculative at this point, we suggest the microglial AT8 signal within CD68-positive volumes could originate from synaptic or ghost tangle phospho tau. Future research should aim to identify the exact structural source of neuronal phospho tau and investigate the implications of phospho tau uptake on microglial functioning.

Part 5: Materials and Methods

Mice & sample isolation

Non-transgenic C57BL6 mice and homozygous Thy1-hP301S Tau mice in a C57BL6 background were maintained at the reMYND NV center (Leuven, Belgium) and brain sections were donated to the VUMC. All housing and experiments were reviewed by the VUMC ethical board and in accordance with the NIH guidelines concerning humane treatment of animals. Mice were kept in cages with 12-hour light/dark cycles and food and water was available *ad libitum*. For the different experiments, groups of littermates (n ≥ 8 per group) were sacrificed at 1, 2, 3, 3.5, 4, 4.5, 5, 5.5 and 6 months of age. Mice were anaesthetized with ketamine, xylazin 2%, atropine and saline (4:2.5:1:2.5). Temperature was monitored with a rectal thermometer before anaesthesia and opening the body cavity, and body temperature was maintained accordingly using a heating blanket. Once the body cavity was opened, the left ventricle was punctured for trans-cardial perfusion with a peristaltic pump and ice-cold saline for three minutes (3 ml/min). Simultaneously, the right atrium was cut to allow excess of liquid to escape. Next, the head was removed from the body and brain was isolated from the skull. From every brain, the left hemisphere was post fixed (4%paraformaldehyde (PFA) in Phosphate Buffered Saline (PBS), -80°C) and stored for long term for potential retrieval of mice-specific material. The right hemisphere was post-fixed overnight (4% PFA in PBS, 4°C) and stored in PBS with 0.1% (v/w) sodium azide (4°C) before sectioning. More specifically, per mouse, 5 sagittal sections (40 µm thick) at intervals of 160 µm were collected using a vibratome (VT1200, Leica) and stored in PBS at 4°C for immunohistochemical analysis.

Immunohistochemistry

In order to look at microglial morphology, several markers (the antigens) were visualized through immunohistochemical (the antibodies) stainings of mouse brain sections. Sections were immunostained in a free-floating manner using antibodies for multiple targets (Addendum, Table 1 and 2): (mouse anti-) AT8 for phosphorylated Tau species (1/500, Thermo Scientific Cat. No. MN1020), (rabbit anti-) IBA1 for reactive microglia (1/1000, WAKO Cat. No. 019-19741, WDE1198), (rat anti-) CD68 for lysosomes (1/400, Bio-Rad Cat. No. MCA1957GA), (mouse anti-) Synaptophysin for presynaptic terminals (1/500, Synaptic Systems Cat. No. 101011), (rabbit anti-) PSD95 for post synaptic terminals (1/400, Merck Millipore Cat. No. 1596) and (goat anti-) IBA1 (1/500, Abcam Cat. No. ab5076). All primary antibodies were diluted in a mixture of PBS, 0.5% or 1% TritonX and 5% normal goat serum (in house produced) or 5% normal donkey serum (Jackson Immunoresearch Cat. No. 017-000-121) and incubated for 2 h at room temperature or, alternatively, overnight at 4°C. Primary antibody binding was visualized by incubation with corresponding Alexa Fluor secondary goat anti-rat 647 (Life Technologies Cat. No. A21247)/-rabbit 555 (Life Technologies Cat. No. A21429)/-mouse 488 (Invitrogen Cat. No. A11017) antibodies (all 1/500, diluted in PBS), and Alexa Fluor secondary Donkey anti-mouse 488 (Invitrogen Cat. No. A21202)/-rabbit 647 (Life Technologies Cat. No. A31573)/-goat 555 (Thermo Scientific Cat. No. A21432) antibodies (all 1/500, diluted in PBS) for 1 or 2 h at room temperature.

Microscopy

Stained tissue sections were coated on glass slides and mounted with Mowiol (see Addendum). Sections were then visualized with either a fluorescent microscope or confocal microscope. More specifically, (fluorescent) Zeiss Imaged D2 was used to image sections (10x

magnification) focussed on medial prefrontal cortex, temporal cortex and dentate gyrus. Resulting images were processed with the Leica Application Suite (LAS) software. Confocal imaging was performed with the Nikon A1R microscope and used to image sections (60x magnification) focussed on temporal cortical regions (layer I and II) directly above the dentate gyrus. Resulting images were processed with the NIS elements software.

Morphological Analysis

Images acquired through confocal microscopy and fluorescent microscopy were further analysed for microglia morphological differences using the ImageJ (Fiji) software (Addendum: Microglial sholl analysis, microglial half sholl analysis, Lysosomal analysis). Microglial cells were identified by IBA1 signals, Tau tangles by AT8 signals, lysosomes by CD68 signals and finally cell somas by DAPI. 14 microglia were selected per animal in both non-transgenic and P301S groups of 5.5 months old mice. For the 2- and 4 months old animals (both non- and transgenic), only 6 cells were traced per animal. Cells were randomly selected, but had to meet several inclusion criteria; 1) cells should be completely included within the z-stack borders, 2) cells should not overlap with one another and 3) cells should reside in the 2nd cortical layer and not in the upper layer lacking neuronal somas. All cells were traced manually by going through the z-stack/dimension and resulting 2D-images were used as input to perform (standard Fiji-) sholl analysis on. For the distance correlation analysis, the distance was measured between microglial soma center and the closest nearby AT8+ soma as measured in the stacked/flattened 2D image. Images not containing AT8+ soma were not included in this analysis resulting in 9-14 cells included per animal of 5.5 months old. For the Half sholl analysis on P301S mice, 2D images of microglial tracings were split into 2 halves perpendicular to the measured angle between the measured microglial soma center and the closest AT8+ soma. Again, images without AT8+ soma were excluded from this analysis. Also, cells were excluded when the measured inter-soma angle was between -45° and -135°, resulting in 4-13 cells included per animal of 5.5 months old, with an average of 9 cells per animal. For the half sholl analysis on non-transgenic mice, 14 traced cells per mouse were included and split into a dorsal and ventral half for further analysis. For the lysosomal analysis, 2 sections per animal (n=6 for both P301S- and non-transgenic mice of 5.5 months old and n=5 for 1/2/3/4/6 months old animals) were analysed. The Imaris x64 software (version 9.1.2, Bitplane AG) was used to quantify microglial (IBA1) and lysosomal (CD68) signals (e.g. number of objects, volume per identified object and total volume of all identified objects) in the individual corresponding channels. The lysosomal signal was masked by the microglial signal in order to obtain lysosomal information solely from lysosomes present inside IBA1+ microglia. Total volume of microglial/lysosomal signal was then normalized by the volume of the imaged section (212.81 µm x 212.81 µm x 5 µm x number of z-stacks). Relative lysosomal volume (%) was calculated by dividing total lysosomal volume by the total microglial volume per image. Per animal, all values were averaged from 2 such images. Next, the identified lysosomes were used as a mask to search for AT8 signals inside microglial lysosomes. The relative AT8-volumes (%) was calculated by dividing total AT8 volume by the total lysosomal volume per image. Again, per animal all values were averaged from 2 images.

Statistical Analysis

Prism 7 (Graphpad Software) was used to perform statistical testing of multiple set-ups (as shown in legends of the figures). Before each test, normality or Gaussian distribution of the

data was investigated through Dagostino and Pearson normality test. Non-parametric tests were used when data sets were not normally distributed. Data in figures are shown as mean ± standard error of mean. Significance levels in the graphs are represented by: * ($P<0.05$), ** ($P<0.01$), *** ($P<0.001$) and **** ($P<0.0001$).

Part 6: References

Ahmed T, Van der Jeugd A, Blum D, Galas M-C, D'Hooge R, Buee L & Balschun D (2014) Cognition and hippocampal synaptic plasticity in mice with a homozygous tau deletion. *Neurobiol. Aging* **35:** 2474–2478

Allen B, Ingram E, Takao M, Smith MJ, Jakes R, Virdee K, Yoshida H, Holzer M, Craxton M, Emson PC, Atzori C, Migheli A, Crowther RA, Ghetti B, Spillantini MG & Goedert M (2002) Abundant tau filaments and nonapoptotic neurodegeneration in transgenic mice expressing human P301S tau protein. *J. Neurosci.* **22:** 9340–51

Alzheimer A (1907) Uber eine eigenartige Erkrankung der Hirnrinde. *Allg Zeits Psychiatry Psych. Med.* **64:** 146–148

Ambegaokar SS & Jackson GR (2011) Functional genomic screen and network analysis reveal novel modifiers of tauopathy dissociated from tau phosphorylation. *Hum. Mol. Genet.* **20:** 4947–4977

American Academy of Family Physicians. R, Kertesz A & Knebl JA (1970) American family physician. American Academy of Family Physicians

Andorfer C, Acker CM, Kress Y, Hof PR, Duff K & Davies P (2005) Cell-Cycle Reentry and Cell Death in Transgenic Mice Expressing Nonmutant Human Tau Isoforms. *J. Neurosci.* **25:** 5446–5454

Andreasson KI, Savonenko A, Vidensky S, Goellner JJ, Zhang Y, Shaffer A, Kaufmann WE, Worley PF, Isakson P & Markowska AL (2001) Age-dependent cognitive deficits and neuronal apoptosis in cyclooxygenase-2 transgenic mice. *J. Neurosci.* **21:** 8198–209

Asai H, Ikezu S, Tsunoda S, Medalla M, Luebke J, Haydar T, Wolozin B, Butovsky O, Kügler S & Ikezu T (2015) Depletion of microglia and inhibition of exosome synthesis halt tau propagation. *Nat. Neurosci.* **18:** 1584–1593

Askew K, Li K, Olmos-Alonso A, Garcia-Moreno F, Liang Y, Richardson P, Tipton T, Chapman MA, Riecken K, Beccari S, Sierra A, Molnár Z, Cragg MS, Garaschuk O, Perry VH & Gomez-Nicola D (2017) Coupled Proliferation and Apoptosis Maintain the Rapid Turnover of Microglia in the Adult Brain. *Cell Rep.* **18:** 391–405

Battistin L & Cagnin A (2010) Vascular Cognitive Disorder. A Biological and Clinical Overview. *Neurochem. Res.* **35:** 1933–1938

Bellucci A, Westwood AJ, Ingram E, Casamenti F, Goedert M & Spillantini MG (2004) Induction of Inflammatory Mediators and Microglial Activation in Mice Transgenic for Mutant Human P301S Tau Protein. *Am. J. Pathol.* **165:** 1643–1652

Bennett ML, Bennett FC, Liddelow SA, Ajami B, Zamanian JL, Fernhoff NB, Mulinyawe SB, Bohlen CJ, Adil A, Tucker A, Weissman IL, Chang EF, Li G, Grant GA, Hayden Gephart MG & Barres BA (2016) New tools for studying microglia in the mouse and human CNS. *Proc. Natl. Acad. Sci.* **113:** E1738–E1746

Le Ber I, Camuzat A, Hannequin D, Pasquier F, Guedj E, Rovelet-Lecrux A, Hahn-Barma V, van der Zee J, Clot F, Bakchine S, Puel M, Ghanim M, Lacomblez L, Mikol J, Deramecourt V, Lejeune P, de la Sayette V, Belliard S, Vercelletto M, Meyrignac C, et al (2008) Phenotype variability in progranulin mutation carriers: a clinical, neuropsychological, imaging and genetic study. *Brain* **131:** 732–746

Berg RL & Shaw GR (2013) Laboratory evaluation for vitamin B12 deficiency: the case for cascade testing. *Clin. Med. Res.* **11:** 7–15

Berger Z, Ravikumar B, Menzies FM, Oroz LG, Underwood BR, Pangalos MN, Schmitt I, Wullner U, Evert BO, O'Kane CJ & Rubinsztein DC (2006) Rapamycin alleviates toxicity of different aggregate-prone proteins. *Hum. Mol. Genet.* **15:** 433–442

Bland ST, Beckley JT, Young S, Tsang V, Watkins LR, Maier SF & Bilbo SD (2010) Enduring consequences of early-life infection on glial and neural cell genesis within cognitive regions of the brain. *Brain. Behav. Immun.* **24:** 329–338

Bolós M, Llorens-Martín M, Jurado-Arjona J, Hernández F, Rábano A & Avila J (2015) Direct Evidence of Internalization of Tau by Microglia In Vitro and In Vivo. *J. Alzheimer's Dis.* **50:** 77–87

Bornemann KD, Wiederhold KH, Pauli C, Ermini F, Stalder M, Schnell L, Sommer B, Jucker M & Staufenbiel M (2001) Abeta-induced inflammatory processes in microglia cells of APP23 transgenic mice. *Am. J. Pathol.* **158:** 63–73

Bromley-Brits K, Deng Y & Song W (2011) Morris water maze test for learning and memory deficits in Alzheimer's disease model mice. *J. Vis. Exp.*

Brunnström HR & Englund EM (2009) Cause of death in patients with dementia disorders. *Eur. J. Neurol.* **16:** 488–492

Bugiani O, Murrell JR, Giaccone G, Hasegawa M, Ghigo G, Tabaton M, Morbin M, Primavera A, Carella F, Solaro

C, Grisoli M, Savoiardo M, Spillantini MG, Tagliavini F, Goedert M & Ghetti B (1999) Frontotemporal dementia and corticobasal degeneration in a family with a P301S mutation in tau. *J. Neuropathol. Exp. Neurol.* **58:** 667–77

Burns A & Iliffe S (2009) Alzheimer's disease. *BMJ* **338:** b158

Butovsky O, Jedrychowski MP, Moore CS, Cialic R, Lanser AJ, Gabriely G, Koeglsperger T, Dake B, Wu PM, Doykan CE, Fanek Z, Liu L, Chen Z, Rothstein JD, Ransohoff RM, Gygi SP, Antel JP & Weiner HL (2014) Identification of a unique TGF-β–dependent molecular and functional signature in microglia. *Nat. Neurosci.* **17:** 131–143

Caplan JP & Rabinowitz T (2010) An Approach to the Patient with Cognitive Impairment: Delirium and Dementia. *Med. Clin. North Am.* **94:** 1103–1116

Carmel R (2008) How I treat cobalamin (vitamin B12) deficiency. *Blood* **112:** 2214–21

Carroll MC (2004) The complement system in regulation of adaptive immunity. *Nat. Immunol.* **5:** 981–986

Casano AM, Albert M & Peri F (2016) Developmental Apoptosis Mediates Entry and Positioning of Microglia in the Zebrafish Brain. *Cell Rep.* **16:** 897–906

Chai X, Wu S, Murray TK, Kinley R, Cella C V., Sims H, Buckner N, Hanmer J, Davies P, O'Neill MJ, Hutton ML & Citron M (2011) Passive Immunization with Anti-Tau Antibodies in Two Transgenic Models. *J. Biol. Chem.* **286:** 34457–34467

Cleveland DW, Hwo SY & Kirschner MW (1977a) Purification of tau, a microtubule-associated protein that induces assembly of microtubules from purified tubulin. *J. Mol. Biol.* **116:** 207–25

Cleveland DW, Hwo SY & Kirschner MW (1977b) Physical and chemical properties of purified tau factor and the role of tau in microtubule assembly. *J. Mol. Biol.* **116:** 227–47

Clinton LK, Blurton-Jones M, Myczek K, Trojanowski JQ & LaFerla FM (2010) Synergistic Interactions between Abeta, tau, and alpha-synuclein: acceleration of neuropathology and cognitive decline. *J. Neurosci.* **30:** 7281–9

Colonna M & Butovsky O (2017) Microglia Function in the Central Nervous System During Health and Neurodegeneration. *Annu. Rev. Immunol.* **35:** 441–468

Le Corre S, Klafki HW, Plesnila N, Hubinger G, Obermeier A, Sahagun H, Monse B, Seneci P, Lewis J, Eriksen J, Zehr C, Yue M, McGowan E, Dickson DW, Hutton M & Roder HM (2006) An inhibitor of tau hyperphosphorylation prevents severe motor impairments in tau transgenic mice. *Proc. Natl. Acad. Sci.* **103:** 9673–9678

Cras P, Kawai M, Siedlak S & Perry G (1991) Microglia are associated with the extracellular neurofibrillary tangles of Alzheimer disease. *Brain Res.* **558:** 312–4

Davalos D, Grutzendler J, Yang G, Kim J V, Zuo Y, Jung S, Littman DR, Dustin ML & Gan W-B (2005) ATP mediates rapid microglial response to local brain injury in vivo. *Nat. Neurosci.* **8:** 752–758

Dawson HN, Ferreira A, Eyster M V, Ghoshal N, Binder LI & Vitek MP (2001) Inhibition of neuronal maturation in primary hippocampal neurons from tau deficient mice. *J. Cell Sci.* **114:** 1179–87

Dickson DW, Kouri N, Murray ME & Josephs KA (2011) Neuropathology of frontotemporal lobar degeneration-tau (FTLD-tau). *J. Mol. Neurosci.* **45:** 384–9

Dissing-Olesen L, LeDue JM, Rungta RL, Hefendehl JK, Choi HB & MacVicar BA (2014) Activation of Neuronal NMDA Receptors Triggers Transient ATP-Mediated Microglial Process Outgrowth. *J. Neurosci.* **34:** 10511–10527

Elmore MRP, Najafi AR, Koike MA, Dagher NN, Spangenberg EE, Rice RA, Kitazawa M, Matusow B, Nguyen H, West BL & Green KN (2014) Colony-Stimulating Factor 1 Receptor Signaling Is Necessary for Microglia Viability, Unmasking a Microglia Progenitor Cell in the Adult Brain. *Neuron* **82:** 380–397

Feng G, Mellor RH, Bernstein M, Keller-Peck C, Nguyen QT, Wallace M, Nerbonne JM, Lichtman JW & Sanes JR (2000) Imaging Neuronal Subsets in Transgenic Mice Expressing Multiple Spectral Variants of GFP. *Neuron* **28:** 41–51

Fernández-Arjona M del M, Grondona JM, Granados-Durán P, Fernández-Llebrez P & López-Ávalos MD (2017) Microglia Morphological Categorization in a Rat Model of Neuroinflammation by Hierarchical Cluster and Principal Components Analysis. *Front. Cell. Neurosci.* **11:** 235

Finger EC (2016) Frontotemporal Dementias. *Continuum (Minneap. Minn).* **22:** 464–89

Galatro TF, Holtman IR, Lerario AM, Vainchtein ID, Brouwer N, Sola PR, Veras MM, Pereira TF, Leite REP, Möller T, Wes PD, Sogayar MC, Laman JD, Den Dunnen W, Pasqualucci CA, Oba-Shinjo SM, Boddeke EWGM, Marie SKN & Eggen BJL (2017) Transcriptomic analysis of purified human cortical microglia reveals age-associated changes. *Nat. Neurosci.* **20:** 1162–1171

Gasparini L, Anthony Crowther R, Martin KR, Berg N, Coleman M, Goedert M & Spillantini MG (2011) Tau inclusions in retinal ganglion cells of human P301S tau transgenic mice: Effects on axonal viability.

Neurobiol. Aging **32:** 419–433
Gasparini L, Terni B & Spillantini MG (2007) Frontotemporal Dementia with Tau Pathology. *Neurodegener. Dis.* **4:** 236–253
Gilmore EC & Herrup K (1997) Cortical development: Layers of complexity. *Curr. Biol.* **7:** R231–R234
Ginhoux F, Greter M, Leboeuf M, Nandi S, See P, Gokhan S, Mehler MF, Conway SJ, Ng LG, Stanley ER, Samokhvalov IM & Merad M (2010) Fate Mapping Analysis Reveals That Adult Microglia Derive from Primitive Macrophages. *Science (80-.).* **330:** 841–845
Godbey WT (2014) Cellular Transport. *An Introd. to Biotechnol.***:** 35–64
Goedert M & Jakes R (1990) Expression of separate isoforms of human tau protein: correlation with the tau pattern in brain and effects on tubulin polymerization. *EMBO J.* **9:** 4225–30
Goedert M, Spillantini MG, Jakes R, Rutherford D & Crowther RA (1989) Multiple isoforms of human microtubule-associated protein tau: sequences and localization in neurofibrillary tangles of Alzheimer's disease. *Neuron* **3:** 519–26
Gomez Perdiguero E, Klapproth K, Schulz C, Busch K, Azzoni E, Crozet L, Garner H, Trouillet C, de Bruijn MF, Geissmann F & Rodewald H-R (2015) Tissue-resident macrophages originate from yolk-sac-derived erythro-myeloid progenitors. *Nature* **518:** 547–551
Grabert K, Michoel T, Karavolos MH, Clohisey S, Baillie JK, Stevens MP, Freeman TC, Summers KM & McColl BW (2016) Microglial brain region-dependent diversity and selective regional sensitivities to aging. *Nat. Neurosci.* **19:** 504–16
Hall GF & Patuto BA (2012) Is tau ready for admission to the prion club? *Prion* **6:** 223–33
Hampton DW, Webber DJ, Bilican B, Goedert M, Spillantini MG & Chandran S (2010) Cell-Mediated Neuroprotection in a Mouse Model of Human Tauopathy. *J. Neurosci.* **30:** 9973–9983
Han J, Harris RA & Zhang X-M (2017) An updated assessment of microglia depletion: current concepts and future directions. *Mol. Brain* **10:** 25
Harada A, Oguchi K, Okabe S, Kuno J, Terada S, Ohshima T, Sato-Yoshitake R, Takei Y, Noda T & Hirokawa N (1994) Altered microtubule organization in small-calibre axons of mice lacking tau protein. *Nature* **369:** 488–491
Harrington CR, Storey JMD, Clunas S, Harrington KA, Horsley D, Ishaq A, Kemp SJ, Larch CP, Marshall C, Nicoll SL, Rickard JE, Simpson M, Sinclair JP, Storey LJ & Wischik CM (2015) Cellular Models of Aggregation-dependent Template-directed Proteolysis to Characterize Tau Aggregation Inhibitors for Treatment of Alzheimer Disease. *J. Biol. Chem.* **290:** 10862–10875
Haynes SE, Hollopeter G, Yang G, Kurpius D, Dailey ME, Gan W-B & Julius D (2006) The P2Y12 receptor regulates microglial activation by extracellular nucleotides. *Nat. Neurosci.* **9:** 1512–1519
HICKEY M, GALLANT K, GROSS G, LEVINE M & CHESSELET M (2005) Early behavioral deficits in R6/2 mice suitable for use in preclinical drug testing. *Neurobiol. Dis.* **20:** 1–11
Hogan DB, Fiest KM, Roberts JI, Maxwell CJ, Dykeman J, Pringsheim T, Steeves T, Smith EE, Pearson D & Jetté N (2016) The Prevalence and Incidence of Dementia with Lewy Bodies: a Systematic Review. *Can. J. Neurol. Sci. / J. Can. des Sci. Neurol.* **43:** S83–S95
Holmes BB, DeVos SL, Kfoury N, Li M, Jacks R, Yanamandra K, Ouidja MO, Brodsky FM, Marasa J, Bagchi DP, Kotzbauer PT, Miller TM, Papy-Garcia D & Diamond MI (2013) Heparan sulfate proteoglycans mediate internalization and propagation of specific proteopathic seeds. *Proc. Natl. Acad. Sci.* **110:** E3138–E3147
Holmes BB, Furman JL, Mahan TE, Yamasaki TR, Mirbaha H, Eades WC, Belaygorod L, Cairns NJ, Holtzman DM & Diamond MI (2014) Proteopathic tau seeding predicts tauopathy in vivo. *Proc. Natl. Acad. Sci.* **111:** E4376–E4385
Hua JY & Smith SJ (2004) Neural activity and the dynamics of central nervous system development. *Nat. Neurosci.* **7:** 327–332
Huberman AD, Feller MB & Chapman B (2008) Mechanisms Underlying Development of Visual Maps and Receptive Fields. *Annu. Rev. Neurosci.* **31:** 479–509
Hutton M, Lendon CL, Rizzu P, Baker M, Froelich S, Houlden H, Pickering-Brown S, Chakraverty S, Isaacs A, Grover A, Hackett J, Adamson J, Lincoln S, Dickson D, Davies P, Petersen RC, Stevens M, de Graaff E, Wauters E, van Baren J, et al (1998) Association of missense and 5'-splice-site mutations in tau with the inherited dementia FTDP-17. *Nature* **393:** 702–705
Ishizawa K & Dickson DW (2001) Microglial activation parallels system degeneration in progressive supranuclear palsy and corticobasal degeneration. *J. Neuropathol. Exp. Neurol.* **60:** 647–57
Jameson L, Frey T, Zeeberg B, Dalldorf F & Caplow M (1980) Inhibition of microtubule assembly by phosphorylation of microtubule-associated proteins. *Biochemistry* **19:** 2472–9
Jeong H-K, Ji K, Min K & Joe E-H (2013) Brain inflammation and microglia: facts and misconceptions. *Exp.*

Neurobiol. **22:** 59–67

Kadowaki H, Nishitoh H, Urano F, Sadamitsu C, Matsuzawa A, Takeda K, Masutani H, Yodoi J, Urano Y, Nagano T & Ichijo H (2005) Amyloid β induces neuronal cell death through ROS-mediated ASK1 activation. *Cell Death Differ.* **12:** 19–24

Katz LC & Shatz CJ (1996) Synaptic activity and the construction of cortical circuits. *Science* **274:** 1133–8

Kierdorf K, Erny D, Goldmann T, Sander V, Schulz C, Perdiguero EG, Wieghofer P, Heinrich A, Riemke P, Hölscher C, Müller DN, Luckow B, Brocker T, Debowski K, Fritz G, Opdenakker G, Diefenbach A, Biber K, Heikenwalder M, Geissmann F, et al (2013) Microglia emerge from erythromyeloid precursors via Pu.1- and Irf8-dependent pathways. *Nat. Neurosci.* **16:** 273–280

Kingwell K (2015) Targeting tau acetylation attenuates neurodegeneration. *Nat. Rev. Drug Discov.* **14:** 749–749

Kobayashi K, Hayashi M, Nakano H, Fukutani Y, Sasaki K, Shimazaki M & Koshino Y (2002) Apoptosis of astrocytes with enhanced lysosomal activity and oligodendrocytes in white matter lesions in Alzheimer's disease. *Neuropathol. Appl. Neurobiol.* **28:** 238–51

Kobayashi K, Muramori F, Aoki T, Hayashi M, Miyazu K, Fukutani Y, Mukai M & Koshino F (1998) KP-1 is a marker for extraneuronal neurofibrillary tangles and senile plaques in Alzheimer diseased brains. *Dement. Geriatr. Cogn. Disord.* **9:** 13–9

Le MN, Kim W, Lee S, McKee AC & Hall GF (2012) Multiple mechanisms of extracellular tau spreading in a non-transgenic tauopathy model. *Am. J. Neurodegener. Dis.* **1:** 316–33

Lee J-H, Jeong S-K, Kim BC, Park KW & Dash A (2015) Donepezil across the spectrum of Alzheimer's disease: dose optimization and clinical relevance. *Acta Neurol. Scand.* **131:** 259–267

Lee VM, Balin BJ, Otvos L & Trojanowski JQ (1991) A68: a major subunit of paired helical filaments and derivatized forms of normal Tau. *Science* **251:** 675–8

Lewis J, McGowan E, Rockwood J, Melrose H, Nacharaju P, Van Slegtenhorst M, Gwinn-Hardy K, Murphy MP, Baker M, Yu X, Duff K, Hardy J, Corral A, Lin W-L, Yen S-H, Dickson DW, Davies P & Hutton M (2000) Neurofibrillary tangles, amyotrophy and progressive motor disturbance in mice expressing mutant (P301L) tau protein. *Nat. Genet.* **25:** 402–405

Leyk J, Goldbaum O, Noack M & Richter-Landsberg C (2015) Inhibition of HDAC6 Modifies Tau Inclusion Body Formation and Impairs Autophagic Clearance. *J. Mol. Neurosci.* **55:** 1031–1046

Li Q & Barres BA (2017) Microglia and macrophages in brain homeostasis and disease. *Nat. Rev. Immunol.* **18:** 225–242

Littin K, Acevedo A, Browne W, Edgar J, Mendl M, Owen D, Sherwin C, Würbel H & Nicol C (2008) Towards humane end points: behavioural changes precede clinical signs of disease in a Huntington's disease model. *Proceedings. Biol. Sci.* **275:** 1865–74

Livingston G, Sommerlad A, Orgeta V, Costafreda SG, Huntley J, Ames D, Ballard C, Banerjee S, Burns A, Cohen-Mansfield J, Cooper C, Fox N, Gitlin LN, Howard R, Kales HC, Larson EB, Ritchie K, Rockwood K, Sampson EL, Samus Q, et al (2017) Dementia prevention, intervention, and care. *Lancet (London, England)* **390:** 2673–2734

Long JM, Kalehua AN, Muth NJ, Calhoun ME, Jucker M, Hengemihle JM, Ingram DK & Mouton PR (1998) Stereological analysis of astrocyte and microglia in aging mouse hippocampus. *Neurobiol. Aging* **19:** 497–503

van Lookeren Campagne M, Wiesmann C & Brown EJ (2007) Macrophage complement receptors and pathogen clearance. *Cell. Microbiol.* **9:** 2095–2102

Loy CT, Schofield PR, Turner AM & Kwok JBJ (2014) Genetics of dementia. *Lancet (London, England)* **383:** 828–40

Ludolph AC, Kassubek J, Landwehrmeyer BG, Mandelkow E, Mandelkow E-M, Burn DJ, Caparros-Lefebvre D, Frey KA, de Yebenes JG, Gasser T, Heutink P, Höglinger G, Jamrozik Z, Jellinger KA, Kazantsev A, Kretzschmar H, Lang AE, Litvan I, Lucas JJ, McGeer PL, et al (2009) Tauopathies with parkinsonism: clinical spectrum, neuropathologic basis, biological markers, and treatment options. *Eur. J. Neurol.* **16:** 297–309

Luo W, Liu W, Hu X, Hanna M, Caravaca A & Paul SM (2015) Microglial internalization and degradation of pathological tau is enhanced by an anti-tau monoclonal antibody. *Sci. Rep.* **5:** 11161

Maphis N, Xu G, Kokiko-cochran ON, Cardona A, Ransohoff RM, Lamb BT & Bhaskar K (2015) Loss of tau rescues inflammation-mediated neurodegeneration. *Front. Neurosci.* **9:** 196

McKeith IG, Boeve BF, Dickson DW, Halliday G, Taylor J-P, Weintraub D, Aarsland D, Galvin J, Attems J, Ballard CG, Bayston A, Beach TG, Blanc F, Bohnen N, Bonanni L, Bras J, Brundin P, Burn D, Chen-Plotkin A, Duda JE, et al (2017) Diagnosis and management of dementia with Lewy bodies: Fourth consensus report of the DLB Consortium. *Neurology* **89:** 88–100

Morris M, Maeda S, Vossel K & Mucke L (2011) The Many Faces of Tau. *Neuron* **70:** 410–426

Mosher KI & Wyss-Coray T (2014) Microglial dysfunction in brain aging and Alzheimer's disease. *Biochem. Pharmacol.* **88:** 594–604

Müller WE, Eckert A, Kurz C, Eckert GP & Leuner K (2010) Mitochondrial Dysfunction: Common Final Pathway in Brain Aging and Alzheimer's Disease—Therapeutic Aspects. *Mol. Neurobiol.* **41:** 159–171

Nakanishi H (2003) Microglial Functions and Proteases. *Mol. Neurobiol.* **27:** 163–176

Neumann H, Kotter MR & Franklin RJM (2008) Debris clearance by microglia: an essential link between degeneration and regeneration. *Brain* **132:** 288–295

Neve RL, Harris P, Kosik KS, Kurnit DM & Donlon TA (1986) Identification of cDNA clones for the human microtubule-associated protein tau and chromosomal localization of the genes for tau and microtubule-associated protein 2. *Mol. Brain Res.* **1:** 271–280

Nixon RA & Yang D-S (2012) Autophagy and neuronal cell death in neurological disorders. *Cold Spring Harb. Perspect. Biol.* **4:**

O'Brien RJ & Wong PC (2011) Amyloid precursor protein processing and Alzheimer's disease. *Annu. Rev. Neurosci.* **34:** 185–204

van Olst L, Bielefeld P, Fitzsimons CP, de Vries HE & Schouten M (2018) Glucocorticoid-mediated modulation of morphological changes associated with aging in microglia. *Aging Cell* **17:** e12790

Ozcelik S, Fraser G, Castets P, Schaeffer V, Skachokova Z, Breu K, Clavaguera F, Sinnreich M, Kappos L, Goedert M, Tolnay M & Winkler DT (2013) Rapamycin Attenuates the Progression of Tau Pathology in P301S Tau Transgenic Mice. *PLoS One* **8:** e62459

Paolicelli RC, Bolasco G, Pagani F, Maggi L, Scianni M, Panzanelli P, Giustetto M, Ferreira TA, Guiducci E, Dumas L, Ragozzino D & Gross CT (2011) Synaptic Pruning by Microglia Is Necessary for Normal Brain Development. *Science (80-.).* **333:** 1456–1458

Pascual O, Ben Achour S, Rostaing P, Triller A & Bessis A (2012) Microglia activation triggers astrocyte-mediated modulation of excitatory neurotransmission. *Proc. Natl. Acad. Sci. U. S. A.* **109:** E197-205

Polfliet MMJ, van de Veerdonk F, Döpp EA, van Kesteren-Hendrikx EML, van Rooijen N, Dijkstra CD & van den Berg TK (2002) The role of perivascular and meningeal macrophages in experimental allergic encephalomyelitis. *J. Neuroimmunol.* **122:** 1–8

Pont-Lezica L, Beumer W, Colasse S, Drexhage H, Versnel M & Bessis A (2014) Microglia shape corpus callosum axon tract fasciculation: functional impact of prenatal inflammation. *Eur. J. Neurosci.* **39:** 1551–1557

Poorkaj P, Bird TD, Wijsman E, Nemens E, Garruto RM, Anderson L, Andreadis A, Wiederholt WC, Raskind M & Schellenberg GD (1998) Tau is a candidate gene for chromosome 17 frontotemporal dementia. *Ann. Neurol.* **43:** 815–825

Ransohoff RM (2016) How neuroinflammation contributes to neurodegeneration. *Science (80-.).* **353:** 777–783

REIF AE & ALLEN JM (1964) THE AKR THYMIC ANTIGEN AND ITS DISTRIBUTION IN LEUKEMIAS AND NERVOUS TISSUES. *J. Exp. Med.* **120:** 413–33

Réu P, Khosravi A, Bernard S, Mold JE, Salehpour M, Alkass K, Perl S, Tisdale J, Possnert G, Druid H & Frisén J (2017) The Lifespan and Turnover of Microglia in the Human Brain. *Cell Rep.* **20:** 779–784

Riley KP, Snowdon DA & Markesbery WR (2002) Alzheimer's neurofibrillary pathology and the spectrum of cognitive function: Findings from the Nun Study. *Ann. Neurol.* **51:** 567–577

Rock RB, Gekker G, Hu S, Sheng WS, Cheeran M, Lokensgard JR & Peterson PK (2004) Role of microglia in central nervous system infections. *Clin. Microbiol. Rev.* **17:** 942–64, table of contents

Rodriguez-Callejas JD, Fuchs E & Perez-Cruz C (2016) Evidence of Tau Hyperphosphorylation and Dystrophic Microglia in the Common Marmoset. *Front. Aging Neurosci.* **8:** 315

Rubinsztein DC (2006) The roles of intracellular protein-degradation pathways in neurodegeneration. *Nature* **443:** 780–786

Ryan CL, Baranowski DC, Chitramuthu BP, Malik S, Li Z, Cao M, Minotti S, Durham HD, Kay DG, Shaw CA, Bennett HPJ & Bateman A (2009) Progranulin is expressed within motor neurons and promotes neuronal cell survival. *BMC Neurosci.* **10:** 130

Saman S, Kim W, Raya M, Visnick Y, Miro S, Saman S, Jackson B, McKee AC, Alvarez VE, Lee NCY & Hall GF (2012) Exosome-associated tau is secreted in tauopathy models and is selectively phosphorylated in cerebrospinal fluid in early Alzheimer disease. *J. Biol. Chem.* **287:** 3842–9

Sasaki A, Shoji M, Harigaya Y, Kawarabayashi T, Ikeda M, Naito M, Matsubara E, Abe K & Nakazato Y (2002) Amyloid cored plaques in Tg2576 transgenic mice are characterized by giant plaques, slightly activated microglia, and the lack of paired helical filament-typed, dystrophic neurites. *Virchows Arch.* **441:** 358–367

Scattoni ML, Gasparini L, Alleva E, Goedert M, Calamandrei G & Spillantini MG (2010) Early behavioural

markers of disease in P301S tau transgenic mice. *Behav. Brain Res.* **208:** 250–257
Schafer DP, Lehrman EK, Kautzman AG, Koyama R, Mardinly AR, Yamasaki R, Ransohoff RM, Greenberg ME, Barres BA & Stevens B (2012) Microglia Sculpt Postnatal Neural Circuits in an Activity and Complement-Dependent Manner. *Neuron* **74:** 691–705
Schafer DP & Stevens B (2010) Synapse elimination during development and disease: immune molecules take centre stage. *Biochem. Soc. Trans.* **38:** 476–481
Scheff SW & Price DA (2006) Alzheimer's disease-related alterations in synaptic density: neocortex and hippocampus. *J. Alzheimers. Dis.* **9:** 101–15
Schroeder SK, Joly-Amado A, Gordon MN & Morgan D (2016) Tau-Directed Immunotherapy: A Promising Strategy for Treating Alzheimer's Disease and Other Tauopathies. *J. Neuroimmune Pharmacol.* **11:** 9–25
Seibenhener ML & Wooten MC (2015) Use of the Open Field Maze to measure locomotor and anxiety-like behavior in mice. *J. Vis. Exp.***:** e52434
Sheffield LG, Marquis JG & Berman NE (2000) Regional distribution of cortical microglia parallels that of neurofibrillary tangles in Alzheimer's disease. *Neurosci. Lett.* **285:** 165–8
Shiotsuki H, Yoshimi K, Shimo Y, Funayama M, Takamatsu Y, Ikeda K, Takahashi R, Kitazawa S & Hattori N (2010) A rotarod test for evaluation of motor skill learning. *J. Neurosci. Methods* **189:** 180–185
Sierra A, Encinas JM, Deudero JJP, Chancey JH, Enikolopov G, Overstreet-Wadiche LS, Tsirka SE & Maletic-Savatic M (2010) Microglia Shape Adult Hippocampal Neurogenesis through Apoptosis-Coupled Phagocytosis. *Cell Stem Cell* **7:** 483–495
Šimić G, Babić Leko M, Wray S, Harrington C, Delalle I, Jovanov-Milošević N, Bažadona D, Buée L, de Silva R, Di Giovanni G, Wischik C & Hof P (2016) Tau Protein Hyperphosphorylation and Aggregation in Alzheimer's Disease and Other Tauopathies, and Possible Neuroprotective Strategies. *Biomolecules* **6:** 6
Snowden JS, Neary D & Mann DMA (2002) Frontotemporal dementia. *Br. J. Psychiatry* **180:** 140–3
Sperfeld AD, Collatz MB, Baier H, Palmbach M, Storch A, Schwarz J, Tatsch K, Reske S, Joosse M, Heutink P & Ludolph AC (1999) FTDP-17: an early-onset phenotype with parkinsonism and epileptic seizures caused by a novel mutation. *Ann. Neurol.* **46:** 708–15
Spillantini MG & Goedert M (2013) Tau pathology and neurodegeneration. *Lancet Neurol.* **12:** 609–622
Spillantini MG, Murrell JR, Goedert M, Farlow MR, Klug A & Ghetti B (1998) Mutation in the tau gene in familial multiple system tauopathy with presenile dementia. *Proc. Natl. Acad. Sci. U. S. A.* **95:** 7737–41
Stevens B, Allen NJ, Vazquez LE, Howell GR, Christopherson KS, Nouri N, Micheva KD, Mehalow AK, Huberman AD, Stafford B, Sher A, Litke AM, Lambris JD, Smith SJ, John SWM & Barres BA (2007) The Classical Complement Cascade Mediates CNS Synapse Elimination. *Cell* **131:** 1164–1178
Stone JG, Siedlak SL, Tabaton M, Hirano A, Castellani RJ, Santocanale C, Perry G, Smith MA, Zhu X & Lee H (2011) The cell cycle regulator phosphorylated retinoblastoma protein is associated with tau pathology in several tauopathies. *J. Neuropathol. Exp. Neurol.* **70:** 578–87
Streit WJ, Braak H, Xue Q-S & Bechmann I (2009) Dystrophic (senescent) rather than activated microglial cells are associated with tau pathology and likely precede neurodegeneration in Alzheimer's disease. *Acta Neuropathol.* **118:** 475–485
Sultan A, Nesslany F, Violet M, Bégard S, Loyens A, Talahari S, Mansuroglu Z, Marzin D, Sergeant N, Humez S, Colin M, Bonnefoy E, Buée L & Galas M-C (2011) Nuclear Tau, a Key Player in Neuronal DNA Protection. *J. Biol. Chem.* **286:** 4566–4575
Swaffer K What the hell happened to my brain? : living beyond dementia
Swerdlow RH & Khan SM (2004) A 'mitochondrial cascade hypothesis' for sporadic Alzheimer's disease. *Med. Hypotheses* **63:** 8–20
Takei Y, Teng J, Harada A & Hirokawa N (2000) Defects in axonal elongation and neuronal migration in mice with disrupted tau and map1b genes. *J. Cell Biol.* **150:** 989–1000
Tang Y & Le W (2016) Differential Roles of M1 and M2 Microglia in Neurodegenerative Diseases. *Mol. Neurobiol.* **53:** 1181–1194
Tatebayashi Y, Miyasaka T, Chui D-H, Akagi T, Mishima K -i., Iwasaki K, Fujiwara M, Tanemura K, Murayama M, Ishiguro K, Planel E, Sato S, Hashikawa T & Takashima A (2002) Tau filament formation and associative memory deficit in aged mice expressing mutant (R406W) human tau. *Proc. Natl. Acad. Sci.* **99:** 13896–13901
Tremblay M-È, Lowery RL & Majewska AK (2010) Microglial Interactions with Synapses Are Modulated by Visual Experience. *PLoS Biol.* **8:** e1000527
Tremblay M-E, Stevens B, Sierra A, Wake H, Bessis A & Nimmerjahn A (2011) The Role of Microglia in the Healthy Brain. *J. Neurosci.* **31:** 16064–16069
Tremblay M-È, Zettel ML, Ison JR, Allen PD & Majewska AK (2012) Effects of aging and sensory loss on glial cells

in mouse visual and auditory cortices. *Glia* **60:** 541–558
Troquier L, Caillierez R, Burnouf S, Fernandez-Gomez FJ, Grosjean M-E, Zommer N, Sergeant N, Schraen-Maschke S, Blum D & Buee L (2012) Targeting phospho-Ser422 by active Tau Immunotherapy in the THYTau22 mouse model: a suitable therapeutic approach. *Curr. Alzheimer Res.* **9:** 397–405
Varghese M, Ho L, Wang J, Zhao W, Levine S, Ono K, Mannino S & Pasinetti G (2014) Green coffee as a novel agent for Alzheimer's disease prevention by attenuating diabetes. *Transl. Neurosci.* **5:**
Vaughan DW & Peters A (1974) Neuroglial cells in the cerebral cortex of rats from young adulthood to old age: an electron microscope study. *J. Neurocytol.* **3:** 405–29
Walker DG & Lue L-F (2015) Immune phenotypes of microglia in human neurodegenerative disease: challenges to detecting microglial polarization in human brains. *Alzheimers. Res. Ther.* **7:** 56
Wang J-Z, Grundke-Iqbal I & Iqbal K (2007) Kinases and phosphatases and tau sites involved in Alzheimer neurofibrillary degeneration. *Eur. J. Neurosci.* **25:** 59–68
Wang L-N, Zhu M-W, Feng Y-Q & Wang J-H (2006) Pick's disease with Pick bodies combined with progressive supranuclear palsy without tuft-shaped astrocytes: A clinical, neuroradiologic and pathological study of an autopsied case. *Neuropathology* **26:** 222–230
Wang Y, Martinez-Vicente M, Krüger U, Kaushik S, Wong E, Mandelkow E-M, Cuervo AM & Mandelkow E (2009) Tau fragmentation, aggregation and clearance: the dual role of lysosomal processing. *Hum. Mol. Genet.* **18:** 4153–4170
Wegmann S, Schöler J, Bippes CA, Mandelkow E & Muller DJ (2011) Competing interactions stabilize pro- and anti-aggregant conformations of human Tau. *J. Biol. Chem.* **286:** 20512–24
Weingarten MD, Lockwood AH, Hwo SY & Kirschner MW (1975) A protein factor essential for microtubule assembly. *Proc. Natl. Acad. Sci. U. S. A.* **72:** 1858–62
Williamson LL, Sholar PW, Mistry RS, Smith SH & Bilbo SD (2011) Microglia and memory: modulation by early-life infection. *J. Neurosci.* **31:** 15511–21
Wischik CM, Harrington CR & Storey JMD (2014) Tau-aggregation inhibitor therapy for Alzheimer's disease. *Biochem. Pharmacol.* **88:** 529–539
Wong AM, Patel N V., Patel NK, Wei M, Morgan TE, de Beer MC, de Villiers WJS & Finch CE (2005) Macrosialin increases during normal brain aging are attenuated by caloric restriction. *Neurosci. Lett.* **390:** 76–80
www.alzforum.org, Thy1.P301S Available at: https://www.alzforum.org/research-models/htaup301s [Accessed July 4, 2018]
www.bioarctic.se Available at: https://www.bioarctic.se/en/alzheimers-disease-2541/ [Accessed July 13, 2018]
www.ghr.nlm.nih.gov Available at: https://ghr.nlm.nih.gov/condition/frontotemporal-dementia-with-parkinsonism-17 [Accessed July 14, 2018a]
www.ghr.nlm.nih.gov Available at: https://ghr.nlm.nih.gov/condition/grn-related-frontotemporal-dementia [Accessed July 16, 2018b]
www.who.int, 12 December 2017 Available at: http://www.who.int/mental_health/neurology/dementia/action_plan_2017_2025/en/ [Accessed July 3, 2018]
Xu H, Rösler TW, Carlsson T, de Andrade A, Bruch J, Höllerhage M, Oertel WH & Höglinger GU (2014) Memory deficits correlate with tau and spine pathology in P301S MAPT transgenic mice. *Neuropathol. Appl. Neurobiol.* **40:** 833–843
Xu J, Wang T, Wu Y, Jin W & Wen Z (2016) Microglia Colonization of Developing Zebrafish Midbrain Is Promoted by Apoptotic Neuron and Lysophosphatidylcholine. *Dev. Cell* **38:** 214–222
Yamanaka M, Ishikawa T, Griep A, Axt D, Kummer MP & Heneka MT (2012) PPAR /RXR -Induced and CD36-Mediated Microglial Amyloid- Phagocytosis Results in Cognitive Improvement in Amyloid Precursor Protein/Presenilin 1 Mice. *J. Neurosci.* **32:** 17321–17331
Yamasaki R, Lu H, Butovsky O, Ohno N, Rietsch AM, Cialic R, Wu PM, Doykan CE, Lin J, Cotleur AC, Kidd G, Zorlu MM, Sun N, Hu W, Liu L, Lee J-C, Taylor SE, Uehlein L, Dixon D, Gu J, et al (2014) Differential roles of microglia and monocytes in the inflamed central nervous system. *J. Exp. Med.* **211:** 1533–49
Yoshiyama Y, Higuchi M, Zhang B, Huang S-M, Iwata N, Saido TC, Maeda J, Suhara T, Trojanowski JQ & Lee VM-Y (2007) Synapse Loss and Microglial Activation Precede Tangles in a P301S Tauopathy Mouse Model. *Neuron* **53:** 337–351
Zilka N, Stozicka Z, Kovac A, Pilipcinec E, Bugos O & Novak M (2009) Human misfolded truncated tau protein promotes activation of microglia and leukocyte infiltration in the transgenic rat model of tauopathy. *J. Neuroimmunol.* **209:** 16–25

Part 7: Addendum

Table 1. Immunohistochemistry staining for IBA1, AT8 and CD68. Sections were stored before use in PBS with 5 mM azide at 4°C**.** The different steps for this free-floating staining are described step-by-step. The spatio-temporal phospho tau analysis was performed using the same protocol, but omitting the anti-Iba1 and anti-CD68 primary and associated secondary antibodies. The antibody-mix[1] (used to dilute primary antibodies) consists of PBS, 0.5% TritonX and 5% normal goat serum (produced in house). PBS=Phosphate Buffered Saline; RT=Room Temperature; ON=Over Night.

- Wash sections 4x in PBS (5 min at RT)
- Block sections with 1 ml antibody-mix[1] (60 min at RT)
- Incubate sections with primary rat anti-CD68 antibody (1/400, Bio-Rad Cat. No. MCA1957GA) in 1 ml antibody mix (2 h at RT)
- Wash sections 4x in PBS (5 min at RT)
- Incubate sections with secondary Goat-anti-Rat 647 antibody (1/500, Life Technologies Cat. No. A21247) in 1 ml PBS (1 h at RT)
- Wash sections 4x in PBS (5 min at RT)
- Incubate sections with primary rabbit anti-IBA1 (1/1000, WAKO Cat. No. 019-19741, WDE1198) and mouse anti-AT8 (1/500, Thermo Scientific Cat. No. MN1020) antibodies, both pooled in 1 ml antibody-mix (ON at 4°C)
- Wash sections 4x in PBS (5 min at RT)
- Incubate sections with secondary Goat-anti-Rabbit 555 (1/500, Life Technologies Cat. No. A21429) and Goat-anti-Mouse 488 (1/500, Invitrogen Cat. No. A11017) both pooled in 1 ml PBS (1 h at RT)
- Wash sections 2x in PBS (5 min at RT)
- Retrieve sections on a glass slide (Thermo Scientific, Cat. No. 12362098, in-house coated with 1% gelatin) and mount with Mowiol mounting medium (Sigma Aldrich Merck, Cat. No. 81381) and a cover glass (Thermo Scientific, Cat. No. 11778691).

Microglial sholl analysis

Images acquired through confocal microscopy and processed with NIS software were further analysed for microglial morphological differences using the ImageJ 7 (Fiji) software. All images were split into red (IBA1), green (AT8), blue (DAPI) and white (CD68) channels. For the microglial morphology analysis, only the red channel was selected. Before tracing, overall brightness and contrast thresholds were determined, based on validating threshold levels for 4 images of non-transgenic and P301S mice. For these randomly selected images, an ideal lower threshold of 0 and upper threshold of 1200 was identified and also used for analysing all other images. Next, for every image, the red channel was used to create a stacked image through maximal intensity Z axis projection. This stacked image is the image on which the individually selected cells are traced/drawn. Inclusion criteria for microglia are described in the Material and Methods section. Cells and processes were manually drawn with the overlay brush (width=1, color=white, transparency=0%) and guided by following the direction/flow of processes of individual cells by going through the z-stack layers of non-stacked images of the

red channel. Processes were traced starting from the soma surface on. Additionally, the soma center of every traced microglial cell was determined arbitrarily and indicated by a single white dot using the overlay brush. For further identification, every traced cell was assigned a number by drawing the number nearby the cell. This resulting image was saved as a .jpeg file. This image was then converted into a (near) binary image by first changing the image to an 8bit format and reducing the brightness and contrast threshold (lower threshold 0, upper threshold 160) until a complete black image is created with only white traced microglial processes, soma center and identification number remaining. For the sholl analysis, it is important cell processes do not overlap and microglial tracings should be distant enough from one another as not to enter each other's maximal radius circle. To this end, tracings from the cells were moved around the image to optimize spread in between them. Additionally, the tracings were moved away from the image edges as these interfere the sholl analysis. The resulting image was rescaled (512 pixels into 212.81 µm units), Inverted and flattened to create a single layer image. As these removed some of the earlier settings, the image was again converted into an 8bit image and threshold set to 0-160 (lower to upper limit). For every analysed image, this final resulting .tif file was saved and used for the regular sholl and half sholl analysis. Next, the straight-line tool was used to draw a line from the soma center (indicated by a white dot) towards the furthest process end and the sholl analysis was performed. Specific settings were used: a starting radius of 2 micrometer away from the soma center, a maximum radius equal to the length of the drawn straight-line tool and a radius step size of 1 µm. Also, an "intersection mask" was created to visually check if the sholl analysis was performed on the completely traced cell and not on neighbouring traced cells. The sholl analysis output was copied to excel files and the number of intersections (interpreted as the number of processes at a set distance from the soma) was further analysed using Graphpad Prism 7. For these analysis, intersections measured within 5 µm from the soma center were excluded as these values were biased by the large soma.

Microglial Half sholl analysis

For every traced cell from P301S mice, the distance and angle was measured from the soma center to the closest nearby AT8+ tangle, using the straight-line tool in Fiji. Images not containing AT8+ tangles were excluded from further analysis. The .tif files created for the full sholl analysis were also used for the half sholl analysis. For every individually traced cell, the measured angle between soma center and closest nearby AT8+ tangle was used to divide every tracing into 2 halves split by a line going through the soma center dot and perpendicular to the earlier measured angle. This way, one half was directly facing the AT8+ tangle and the other half was facing the opposite side. Both sides were then used as input for a sholl analysis using the same settings as described earlier. Again, these results were saved in excel files and further analysed using Graphpad Prism 7. The measured distance from soma center to the closest nearby AT8+ tangle was also used for a distance correlation analysis with the microglial morphological complexity (Distance correlation aanlysis) using Graphpad Prism 7.

Lysosomal Analysis

Images acquired through confocal microscopy and processed with the NIS software were further analysed for lysosomal content differences using the Imaris x64 software (version 9.1.2) from Bitplane AG. All images were first converted into imaris image files using the "file converter function" of imaris. First, surfaces were created to mimic the microglial cells using

the “surface” function (settings: IBA1 channel, not smooth, threshold 750, without splitting touching objects, minimum volume threshold of 10 pixels). The lysosomal signals were masked by the newly created microglial surfaces using the “mask all” function. Next, the surfaces of masked lysosomal signals were created using the “surface” function (masked CD68 channel, not smooth, threshold 150, without splitting touching objects, minimum volume threshold of 5 pixels). For both the microglial and lysosomal signals, thresholds were determined by manually adjusting thresholds to simulate the original image, for 3 images per condition. Total volume of microglial/lysosomal signal was then normalized by the volume of the imaged section (212.81 µm x 212.81 µm x 5 µm x number of z-stacks). Relative lysosomal volume (%) was calculated by dividing total lysosomal volume by the total microglial volume per image. Per animal, all values were averaged from 2 such pictures. Next, AT8 signals potentially inside lysosomes were masked by the lysosomal surfaces using the “mask all” function. The surface of these masked AT8 signals were then created using the “surface” function (masked AT8 channel, not smooth, threshold 1000, without splitting touching objects, minimum volume threshold of 0.1 um^3). Finally, for the microglial, lysosomal and AT8 surfaces, data (volume (um^3) per identified object) was extracted in excel files and used as input in Graphpad Prism7 for further analysis and statistical testing.

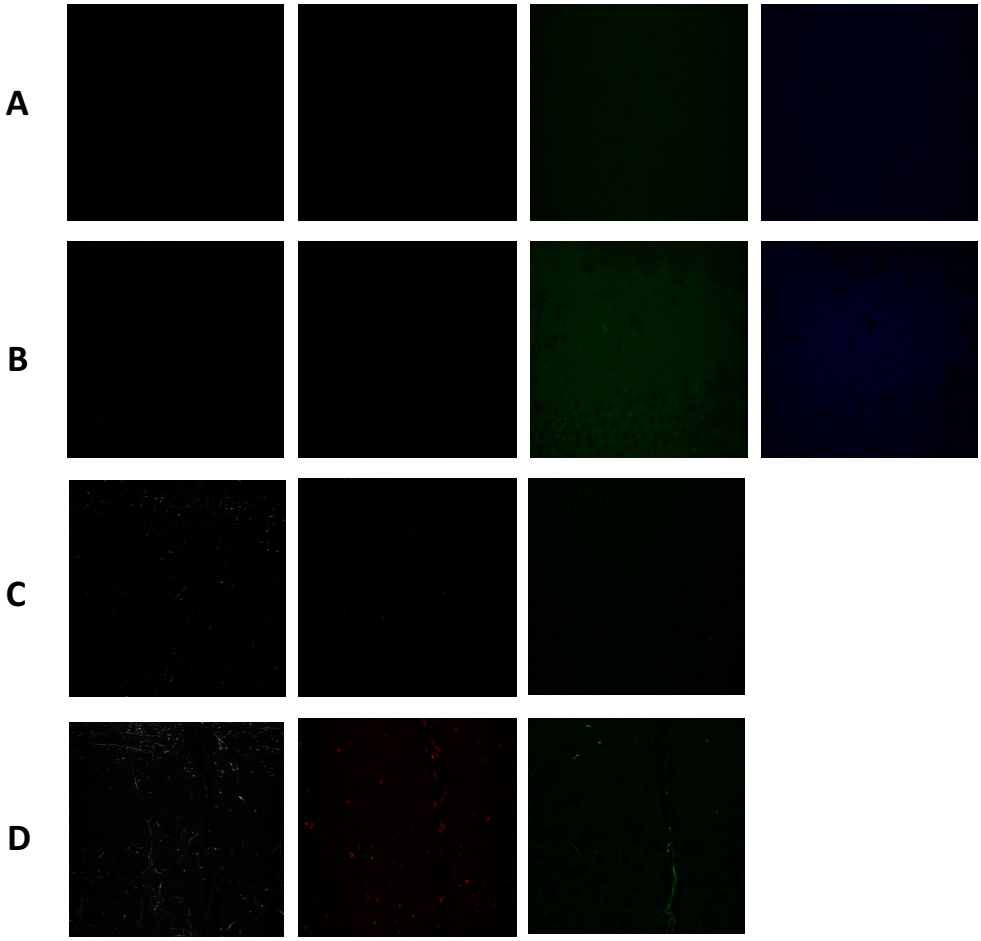


Figure 15. Autofluorescence and antibody specificity during immunohistochemical staining. Representative photomicrographs depicting autofluorescence and secondary antibody specificities in cortical regions of sagittal brain sections of 5.5 months old A and C) Thy1-hTau.P301S and B and D) non-transgenic mice, imaged through confocal imaging (60X magnification). A and B) Shown are autofluorescent signals at wave lengths of (from left to right): 647 nm, 555 nm, 488 nm and 445 nm. Secondary antibody specificity is shown in C) and D), as all primary antibodies were omitted during the staining and shown (from left to right) at wave lengths of: 647 nm, 555 nm and 488 nm.

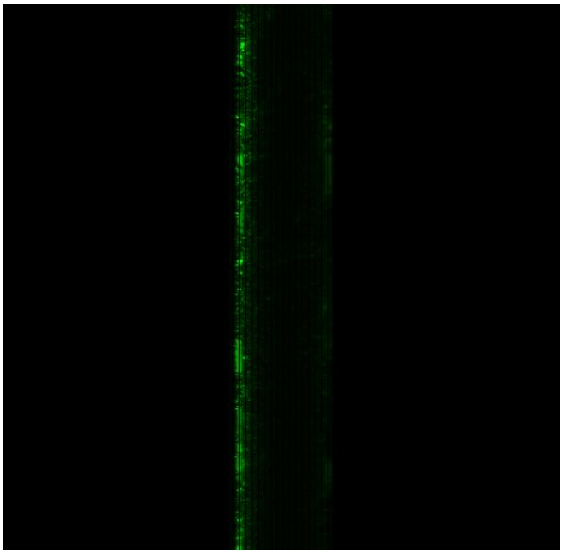


Figure 16. Non-optimal penetration of the AT8 (phospho tau) antibody. Representative photomicrograph depicting phospho tau signals inside an immunohistochemically stained sagittal tissue sections of 5.5 months old P301S mice. Cortical regions were imaged through confocal imaging (60X magnification) and resulting 3D image was generated with Fiji. The imaged block was turned 90 degrees around its center, and the resulting side-view shows the complete depth (about 40 µm) of the tissue section.